STUDY THE EFFECT OF STRIPE HEIGHT AND READ TRACK WIDTH ON BLOCKING TEMPERATURE

CHAYAPIM KULPROMSARO

A THESIS SUBMITTED IN PARTIAL FULFILLMENT

OF THE REQUIREMENT FOR THE DEGREE OF

MASTER OF ENGINEERING IN DATA STORAGE TECHNOLOGY

INTERNATIONAL COLLEGE

KING MONGKUT'S INSTITUTE OF TECHNOLOGY LADKRABANG

2014

KMITL-2014-IC-M-005-005

STUDY THE EFFECT OF STRIPE HEIGHT AND READ TRACK WIDTH ON BLOCKING TEMPERATURE

CHAYAPIM KULPROMSARO

A THESIS SUBMITTED IN PARTIAL FULFILLMENT
OF THE REQUIREMENT FOR THE DEGREE OF
MASTER OF ENGINEERING IN DATA STORAGE TECHNOLOGY
INTERNATIONAL COLLEGE
KING MONGKUT'S INSTITUTE OF TECHNOLOGY LADKRABANG
2014

KMITL-2014-IC-M-005-005

Thesis: Study the effect of stripe height and read track width on blocking temperature
Student: Miss. Chayapim Kulpromsaro
Study ID: 53600606
Degree: Master of Engineering (M.E.)
Program: Data Storage Technology
Year: 2014
Thesis Advisor: Asst.Prof.Dr.Kasin Vichienchom
Co-Advisor: Associate Professor Dr.Wanchai Pijitrojana

ABSTRACT

This thesis describes the study of relationship between the dimensions of read head sensor and its blocking temperature. In this study, blocking temperature of the read head sensor with various stripe heights and read track widths was investigated. QST measurements were performed on the magnetic read head samples to find their critical voltage which was used to calculate the blocking temperatures. The correlation between the read head dimension and the blocking temperature was obtained using statistical analysis. The result shows that the blocking temperature decreases with shorter stripe height. In addition, the analysis reveals that as the read head dimension decreases, its resistance measured during the QST testing increases. Therefore by measuring only resistance, a more simple reliability screening can be done without the need of calculating the blocking temperature which is complicated and time consuming.

Acknowledgement

This work is supported by Western Digital Thailand. I would like to extend my sincere gratitude to my advisor Asst.Prof.Dr.Kasin Vichienchom and Assoc. Professor Dr. Wanchai Pijitrojana for advising me on this research work. I appreciate the thesis committees for their precious time and advice which helped to give an admirable shape to this thesis. I also thank my Supervisors and co-workers for help in all aspects. This accomplishment would not have been possible without the encouragement and support from my family.

Contents

Contents (Cont.)

List of Tables

Page

List of Figures

Page

List of Figure (Cont.)

Page

List of Figure (Cont.)

Page

List of Abbreviation

HDD	Hard Disk Drive
AD	Areal Density
SRC	Storage Research Consortium
NEDO	Energy and Industrial Technology Development Organization
INSIC	Information Storage Industry Consortium
HDI	Head Disk Interface
RTW	Read Track Width
FLTW	Free Layer Track Width
SH	Stripe Height
PL	Pinned layer
RL	Reference layer
FM	Ferromagnetic
PM	Permanent Magnets
AFM	Anti-ferromagnetic
QST	Quasi Static Test
Tb	Blocking Temperature
MTJs	Magnetic Tunnel Junction
TMR	Tunneling Magneto resistance
SDP	Spin-Dependent Tunneling
ELG	Electrical Lapping Guide

Chapter 1
Introduction

1.1 Background

The major components of hard disk drive are disk platter, read/write head, head arm or head slider, head actuator mechanism, spindle motor, logic board, air filter, and cables and connector as showed in Fig. 1.1 Each component is tested by an appropriate approach, such as the electrical performance, the mechanical performance and the reliability. For this study, the reliability of read head is focused.

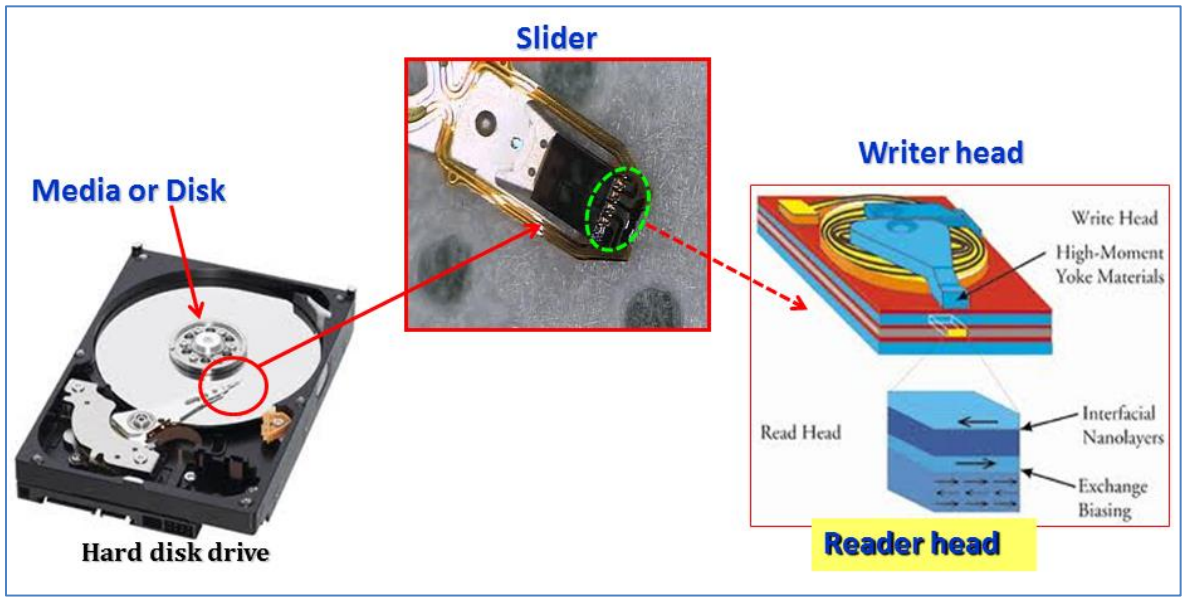

Fig. 1.1 Hard disk drive components.

The Hard Disk Drive Technology has become more effective in terms of saving the cost and the size of areal density. According to Fig. 1.2, the areal density trend and roadmap of the research targeted from the different institutes, has started targeting 2 Tb/in^2 by 2010 for Storage Research Consortium (SRC), 5 Tb/in^2 by 2013 for New Energy and Industrial Technology Development Organization (NEDO), and 10 Tb/in^2 by 2015 for Information Storage Industry Consortium. This study, therefore, focuses on the read head, which is important and also needs to develop in order to reach the roadmap requirement.

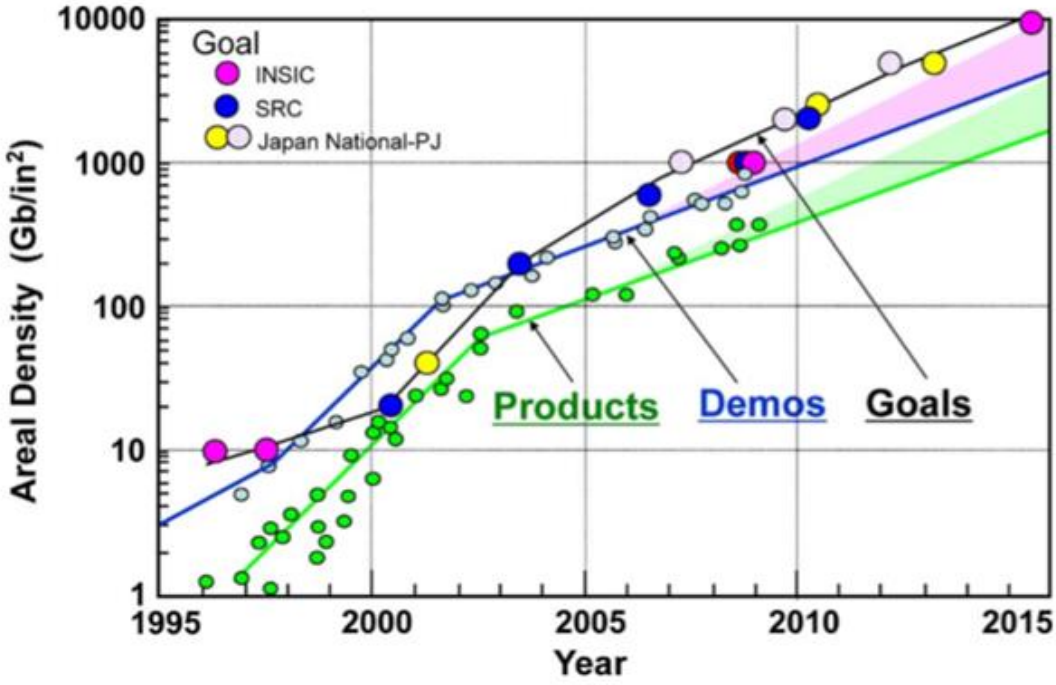

Fig. 1.2 Areal density R&D Targets [1]

1.2 Statement and significance of the problems

The Hard Disk Drive Technology is required high areal density to support the current market need and a higher amount of demand in a long term. Consequently, the magnetic recording head has been designed to become smaller, while increasing the disk capacity. At this point, the areal density of the magnetic recording is continually improved. For a high areal density, a precision control of the read track width and stripe height is required as illustrated in Fig. 1.3.

Regarding the above statement, the thermal stability of exchange bias will be observed, when the read head volume decreases. To clarify, while the hard disk drive is operating, the bias current operation occurs. It leads the temperature of the read head to increase. It is obvious that exchange biasing is strongly dependent on temperature. Admittedly, 'Blocking temperature (T_b)' is a significant temperature level that lets the shift of the hysteresis loop to zero.

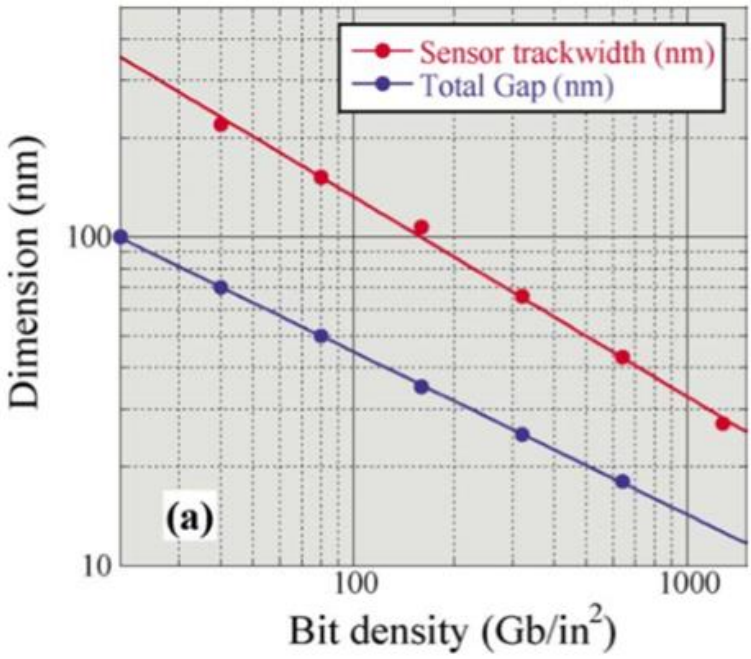

Fig. 1.3 Scaling estimate of head dimensions in terms of recorded bit density (Gbit/in^2). [2]

In order to increase the areal density of magnetic recording, the critical dimensions of recording heads have to be decreased. The blocking temperature (T_b) is a key parameter, which depends on the volume of the magnetic recording read head. Blocking temperature (T_b) is the temperature that the exchange bias property between an antiferromagnetic (AFM) and a ferromagnetic (FM) disappears. Blocking temperature also correlates to the time to failure of the whole hard disk drive. So the blocking temperature is critical for the reliability of the magnetic recording head.

1.3 Objective

The magnetic read head technology is continuously designed to become smaller in order to get the highest areal density. Due to small volume, the thermal stability is investigated for this study. The objective of this research is to study the relationship between the dimension of read head and its blocking temperature (T_b).

1.4 Scope and limitations

For this study, the researcher focuses on the blocking temperature of various magnetic read head physical dimensions, which are read track width (RTW), and stripe height (SH). The scope of the thesis is to investigate the performance of a magnetic read head, specifically for Tunneling Magmatic Resistance (TMR) technology. The key parameter is the blocking temperature, which is measured by Quasi Static Test (QST).

Considering the limitation of this study, the head sensors are fabricated in Western Digital USA plant, so the researcher is not able to change the magnetic material and other designs, excepting the physical dimensions provided by the Western digital Bang Pa-In plant. The read track width and the stripe height ratio are the changeable physical dimensions for this study.

Chapter 2
Literature Review

2.1 The Overview of magnetic tunneling junction (MTJs)

A magnetic tunnel junction (MTJ) is consisted of two ferromagnetic (FM) layers separated by an ultrathin of oxide insulator layer as illustrated in Fig. 2.1. The tunneling current of MTJs depends on the relative magnetizations of the two electrodes, which can be changed by an applied magnetic field. This phenomenon is called 'Tunneling Magneto Resistance' (TMR), which is a consequence of spin-dependent tunneling (SDP). [3], [4]

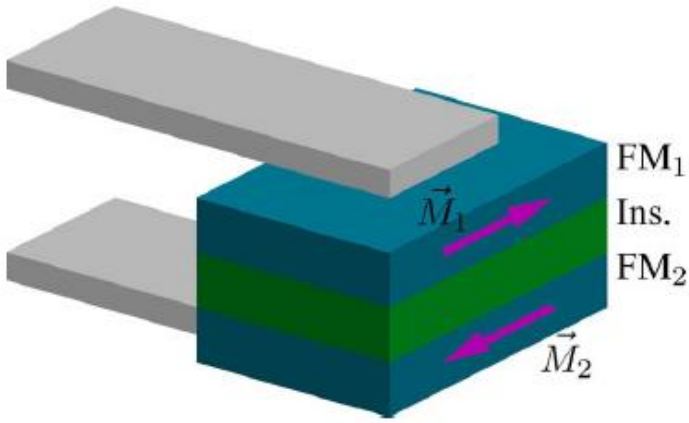

Fig. 2.1 Typical structure of an MTJ

TMR effect can be defined by Julliere's spin-polarized tunneling model as; $TMR = \frac{2P_1P_2}{(1-P_1P_2)}$; where P_1 and P_2 are the spin polarizations of the two electrodes.

If the two FM films are magnetized parallel, the minority spins tunnel to the minority states and the majority spins tunnel to the majority states as show in Fig. 2.2, resulting in a low resistance. However, if the two films are magnetized antiparallel the majority spin and minority spin electrons is reversed, resulting in a high resistance.

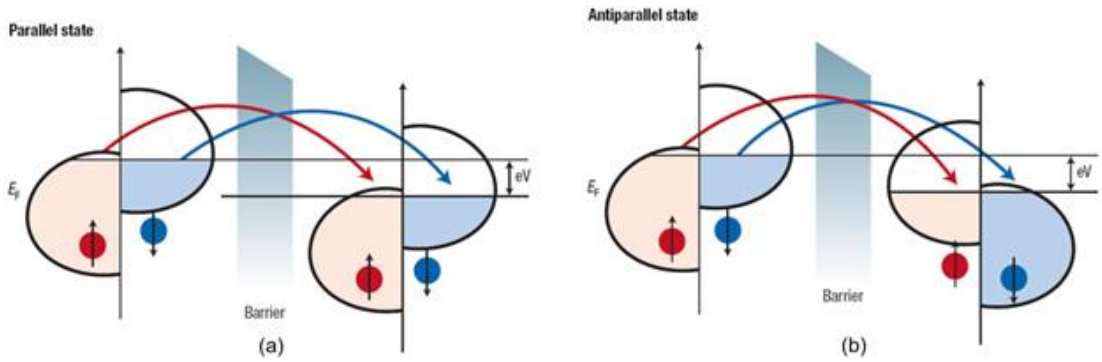

Fig. 2.2 Schematic of the TMR effect in an MTJ
where (a) Parallel state and (b) antiparallel state [2]

2.2 The application of MTJs in HDD read head

MTJs have been widely used in HDD read head application due to high tunneling magnetoresistance (TMR) ratio and low resistance-area (RA) product. The structure of MTJ read head in HDD is consists of antiferromagnetic (AFM) pinning layer/ ferromagnetic pinned (reference) layer/ tunnel barrier/ ferromagnetic free (sense) layer.

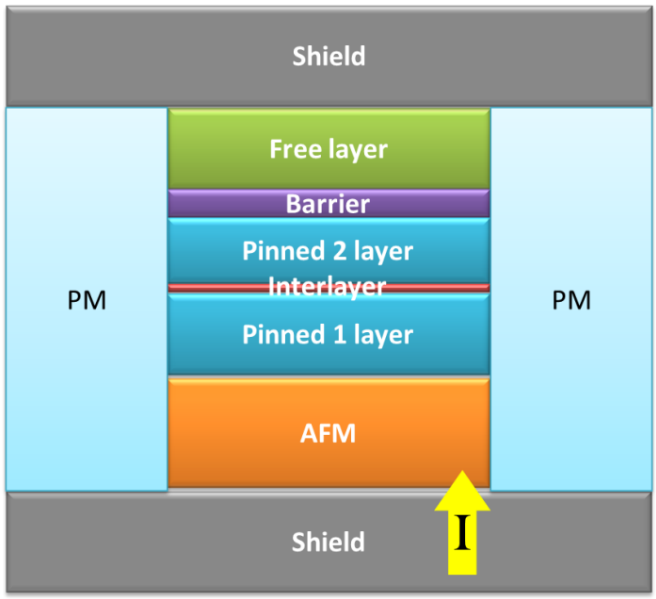

Fig. 2.3 MTJ read head MTJ structure in HDD.

One of the magnetic electrodes of the tunnel junction is the free layer (FL) or sense layer, which magnetic flux from the media in a rotation of its magnetization in response to the flux. The other magnetic electrode is known as the reference layer (RL).

Its magnetization orientation is fixed in the vertical direction to surface of the disk by being next to a multilayered structure consisting of a thin metallic interlayer, a pinned layer (PL), and an antiferromagnetic layer (AFM). The magnetic moment orientation of the pinned layer (PL) is constrained by an effective surface magnetic field, known as an exchange bias field, which arises from the interface with the antiferromagnetic layer (AFM). The purpose of the pinned layer (PL) is to compensate the stray field from the reference layer (RL). Hence, the magnetic moment of the pinned layer (PL) is always opposite to the reference layer (RL). This is done by introducing a strong antiparallel coupling between them by choosing a particular metallic interlayer of sufficient thickness. The resulting tri-layer of the RL/interlayer/PL is often referred to as a synthetic anti-ferromagnetic (SAF). A practical SAF in use is CoFe/Ru/CoFe. Fig.2.3 shows the junction stack is sandwiched in between two soft magnetic shields in the down track direction with a pair of permanent magnets (PM) in the cross track direction maintain the single domain state of the free layer in the MTJ. Fig. 2.4 shows TEM images of MTJ read heads used in present HDD products viewed from the air-bearing surface (ABS).

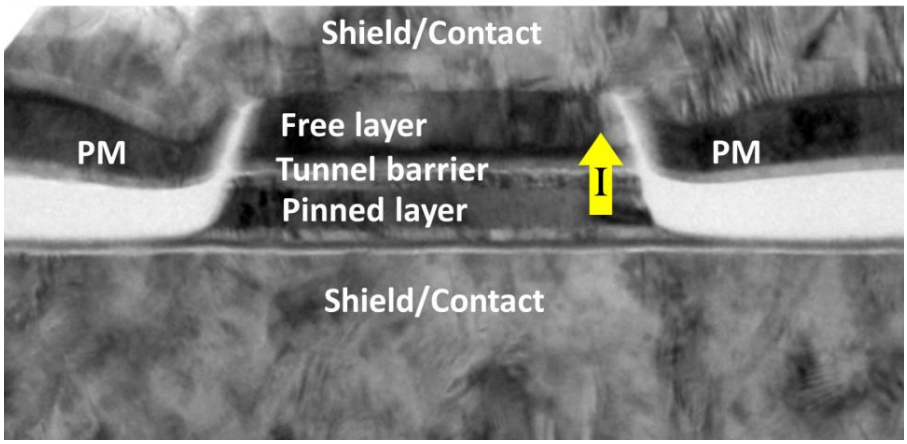

Fig. 2.4 TEM imaged of MTJ read head in an HDD

2.3 The definition of blocking temperature

Since the ambient temperature of TMR head increases with bias current during reading operations, the thermal stability of the exchange biasing is concern for head design and governs the choice of the biasing material. It is well known that exchange biasing is strongly dependent on temperature. At a so-called "blocking temperature" T_b, the exchange field, which is equal to the shift of the hysteresis loop, decreases to zero.

Then, the blocking temperature is the temperature, which the exchange bias between an antiferromagnetic and ferromagnetic disappears. [8]

A blocking temperature (T_b) can be defined as the temperature between the blocked and the superparamagnetic state. [16]

$$T_b = \frac{\Delta E}{k_B \ln(\frac{\tau_m}{\tau_0})} \tag{2.1}$$

Where ΔE is the Energy Barrie.

k_B is the Boltzmann constant.

τ_m is the measurement time.

τ_0 is the length of time characteristic of the probed material.

The energy barrier ΔE occurs in particles with anisotropies. Since those particles' spin shows a preference for certain directions, their energy landscapes contain minima in the preferred directions and maxima in the least preferred directions.

Without external magnetic field, the energy barrier takes the form:

$$\Delta E = KV \tag{2.2}$$

Where K is anisotropy constant.

V is the grain's volume.

From equation (2.1) and (2.2),

$$T_b = \frac{KV}{k_B \ln(\frac{\tau_m}{\tau_0})} \tag{2.3}$$

The grain's volume (V) can be explained as below.

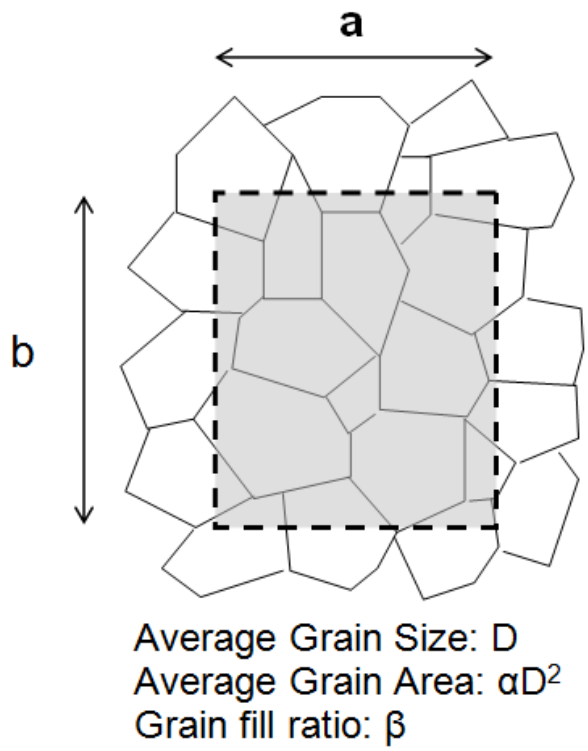

Fig. 2.5 Assumes grains are squares, and fill all the areas. [17]

Number of partial grains the box boundary cuts through: $\frac{2(a+b)}{D}$.

Average area of the partial grains: $\frac{D^2}{2}$.

Total area of partial grains inside the box: $(a+b)D$.

Total area of whole grains inside the box: $ab-(a+b)D$.

Average size of whole grains: D^2.

Number of whole grains inside the box: $\frac{ab-(a+b)D}{D^2}$.

Total number of grains inside the box: $\frac{2(a+b)}{D}+\frac{ab-(a+b)D}{D^2}=\frac{ab+(a+b)D}{D^2}$.

Average area of grains inside the box: $\frac{ab}{\frac{ab+(a+b)D}{D^2}}=D^2\frac{1}{1+\left(\frac{1}{a}+\frac{1}{b}\right)D}$. (2.4)

From equation (2.3) and (2.4), the blocking temperature calculation is:

$$T_b = \frac{K}{k_B \ln\left(\frac{\tau_m}{\tau_0}\right)} \cdot D^2 \frac{1}{1+\left(\frac{1}{a}+\frac{1}{b}\right)D} \tag{2.5}$$

From Fig. 2.5, ***a*** represent to read track width and ***b*** represent to stripe height. An equation (2.5) explains the relation between blocking temperature and magnetic read head especially read track width and stripe height.

The blocking temperature (T_b) testing is proposed to determine the thermal noise stability, which is related to the reliability of the read sensor head. The thermal stability in a hard disk drive is significantly important because it leads to a magnetic structural degradation caused by a diffusion or disorder of a magnetic domain in sensor heads.

Fig. 2.6 shows the magnetic domain direction in an original state. It will reorient to an opposite direction when temperature rises due to an external field stress.

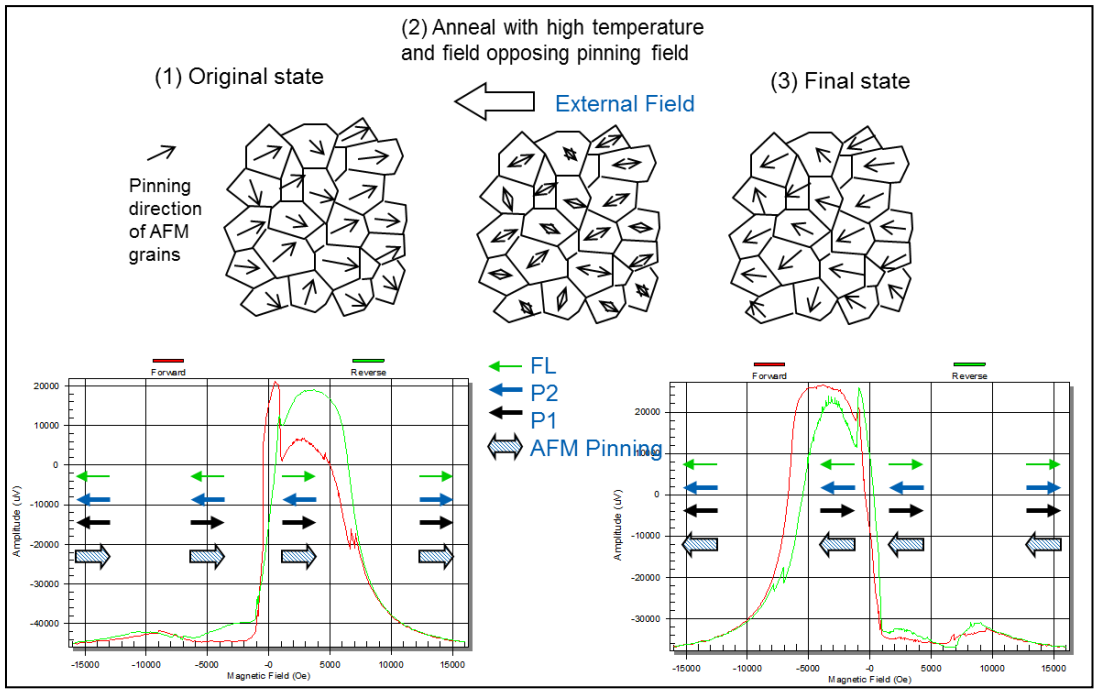

Fig. 2.6 Temperature rises to magnetic domain direction

2.4 The causes of the change of blocking temperature

2.4.1 Magnetic materials [5]

Fig. 2.6 shows the correlation between an expected lifetime and fraction of loose (e.g., unblocked) antiferromagnetic grains in spin-vale sheet films. There are several types of antiferromagnetic layer, such as FeMn, IrMn, PtMn, NiMn, and CrPdMn. According to the graph, the exchange field decreases when the temperature increases. Each type of layer affects different level of temperature.

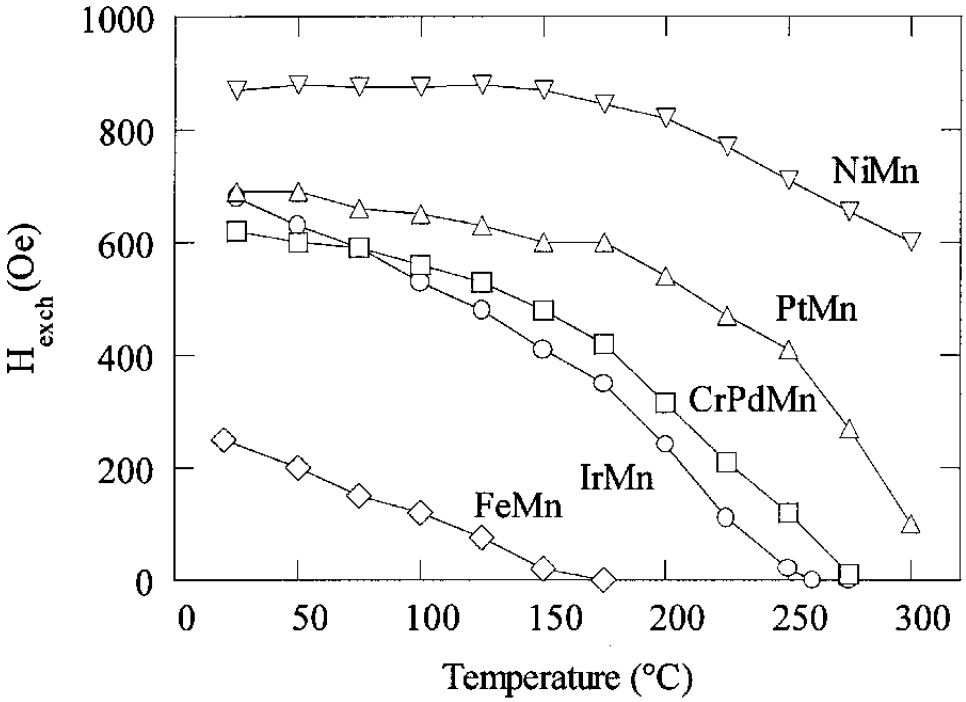

Fig. 2.7 Temperature dependence of the exchange field in spin-valve sheet films with different antiferromagnetic layers. [5]

From Fig. 2.7, it is obvious that NiMn and PtMn are appropriate layers in terms of the thermal stability in recording heads. Both of them show no, or a small fraction of, unblocked grains below 150 °C.

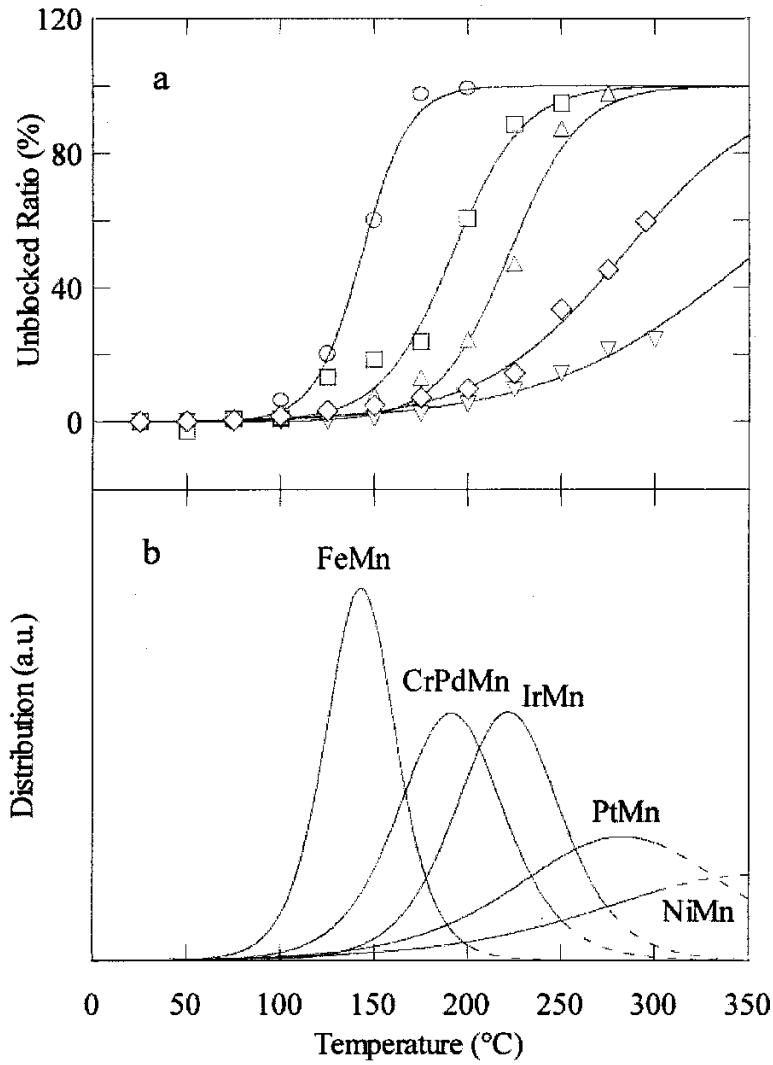

Fig. 2.8 shows the unblocked ratio in spin-valve structures with the different antiferromagnetic layers. The blocking temperature distribution of the different structures studied here is reported in Fig. 2.8 (b). [5]

Clearly, NiMn and PtMn are recognized as the most suitable layers, comparing to the other materials for disk-drive applications. From this study, NiMn and PtMn obviously exhibit sufficient long term stability for disk-drive operations, with expected lifetimes of above 100 years

2.4.2 Thickness of anti-ferromagnetic layer [8], [10]

The change of blocking temperatures of antiferromagnetic / ferromagnetic exchange couples depends on the thickness of antiferromagnetic layer. Fig. 2.9 shows that the blocking temperature increases while antiferromagnetic layer increases.

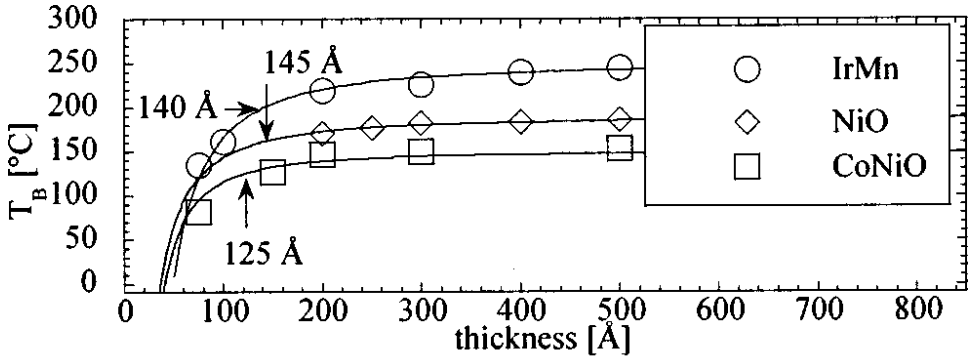

Fig. 2.9 show blocking temperatures while varying thickness of antiferromagnetic layer. [10]

2.4.3 Thickness of ferromagnetic layer [9]

According to Fig. 2.10, the blocking temperature decreases by up to 29%, when ferromagnetic layer thickness is 12nm compared to the sample with the 3 nm ferromagnetic layer. The blocking temperature occurs when the exchange field from the ferromagnetic layer acting on the antiferromagnetic layer is neglected. The thickness of the ferromagnetic layer affects the determination of exchange bias systems. It is clear that the thickness of the ferromagnetic layer increases the exchange field acting on the antiferromagnetic.

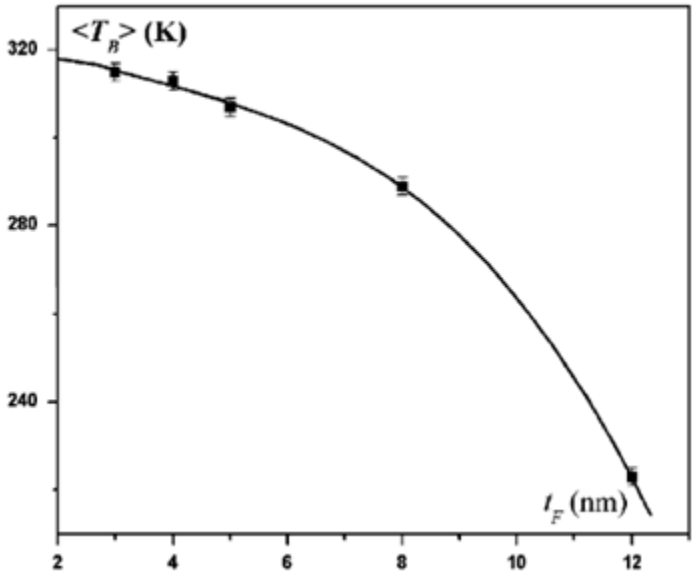

Fig. 2.10 the variation of blocking temperature T_B with the thickness of the ferromagnetic layer t_F (nm) [9]

2.4.4 Deposition condition of antiferromagnetic layer [10]

The graph shows that the deposition of the antiferromagnetic $Co_{0.5}Ni_{0.5}O$ layer used sputtering method. Its approach uses different values of negative substrate bias and pressure.

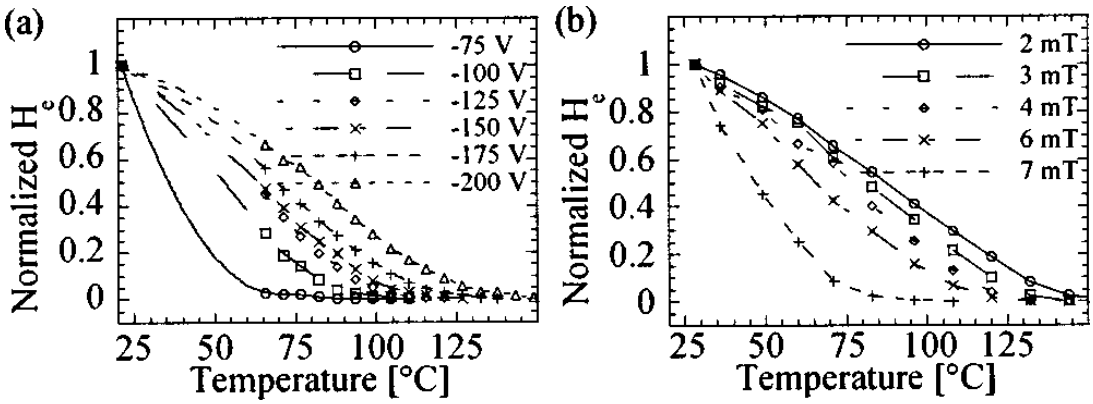

Fig. 2.11 Normalized exchange field as a function of temperature with (a) substrate parameter and (b) pressure as a parameter. [10]

From Fig. 2.11, it can be seen that the blocking temperature, as estimated from the temperature axis intercepts, rises with an increase of negative substrate bias and a decrease sputtering pressure. Using $Co_{0.5}Ni_{0.5}O$ as the material, the deposition condition with high negative substrate biases and low pressures brings about the largest blocking temperatures.

2.5 Conclusion

Many previous studies found that there were many factors impacting on the change of blocking temperature, for instance, magnetic materials [5], a thickness of AFM layer [8], [10], the ferromagnetic layer [9] and deposition conditions of AFM layer [10]. The results show that blocking temperature performance depends on the thickness of AFM and FM layer. If AFM thickness increases while FM's thickness decreases, the blocking temperature will achieve high performance. Additionally, other factors of deposition conditions, which are high negative substrate biases and low pressures, can contribute to the largest blocking temperature.

Most of those studies have focused upon other areas differently to the researcher does. For this study, the researcher will especially explore magnetic read physical dimensions, namely, stipe height (SH) and read track width (RTW).

Chapter 3
Research Methodology

3.1 Purpose

To study blocking temperature on tunneling magnetic read head (TMR) technology when vary stripe height (SH) and read track width (RTW) by using Quasi static test machine (QST).

3.2 Material and method

There are 2 designs of read track width (RTW): 24nm and 27nm. The difference between the samples is the stripe height target (SH): nominal stripe height target (SH), +/-5nm from nominal SH and +/-10nm from nominal SH.

The stripe height target (SH) targets are defined by lapping machine at slider fab process as shown in Fig. 3.1. They are built in head gimbal assembly (HGA) form.

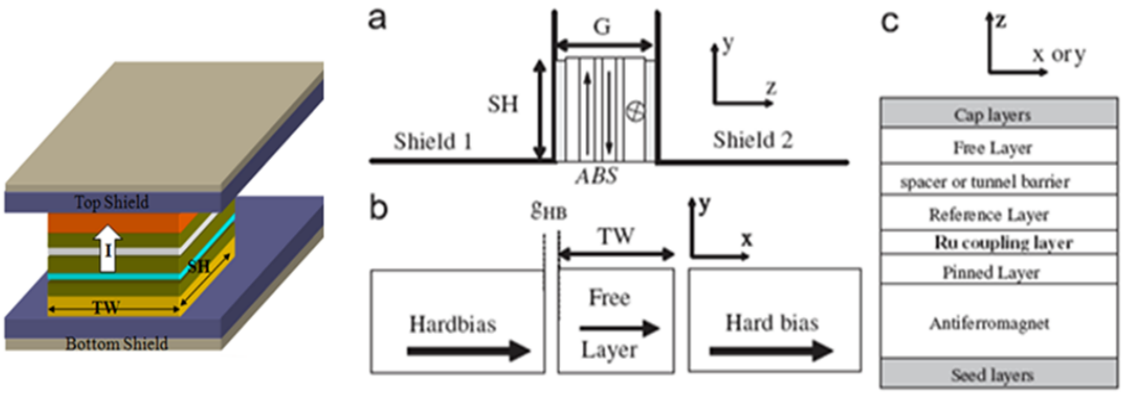

Fig. 3.1 Structure of TMR material, (a) device cross-section. (b) hard bias (permanent magnet) stabilization of free layer. (c) generic CPP stack. [14]

3.2.1 Slider fab process flow.

SF Process can be separated to 3 main parts as shown in Fig. 3.2, Blue blocks represent Front End, yellow and gray blocks represent Clean room operation and pink blocks represent Back End process.

Front End operation starts from loading wafer into strip height grinding process, bar will be divided then lapped on back side to get suitable bar thickness and stress management. The most important operation is the lapping process. There are 2 steps, rough and fine lapping processes. We need to define electrical lapping guide (ELG) resistance targets as both steps for different SH. ELG resistance calculated from below equation.

$$\mathbf{SH = (Slope \times ELG) + Intercept}$$

Where slope is the sensitivity of magnetic material to SH, intercept is the offset between ELG and Read sensor.

Clean room operation starts from DLC FCA process. The purpose is to coat ABS surface with diamond like carbon (DLC) to protect magnetic sensor stripe height. There are 4^{th} steps of Photo Lithography processes then finish clean room operation.

Back End operation starts with TIP-debond, Automate cleaning, Row bond, Head Part and Robot sort before performs the electrical performance measurement at quasi static tester (QST). Finished sliders are separated by Robot sort as per electrical performance from QST. The final operations are automatic cleaning process and appearance inspection at air bearing surface (ABS inspection).

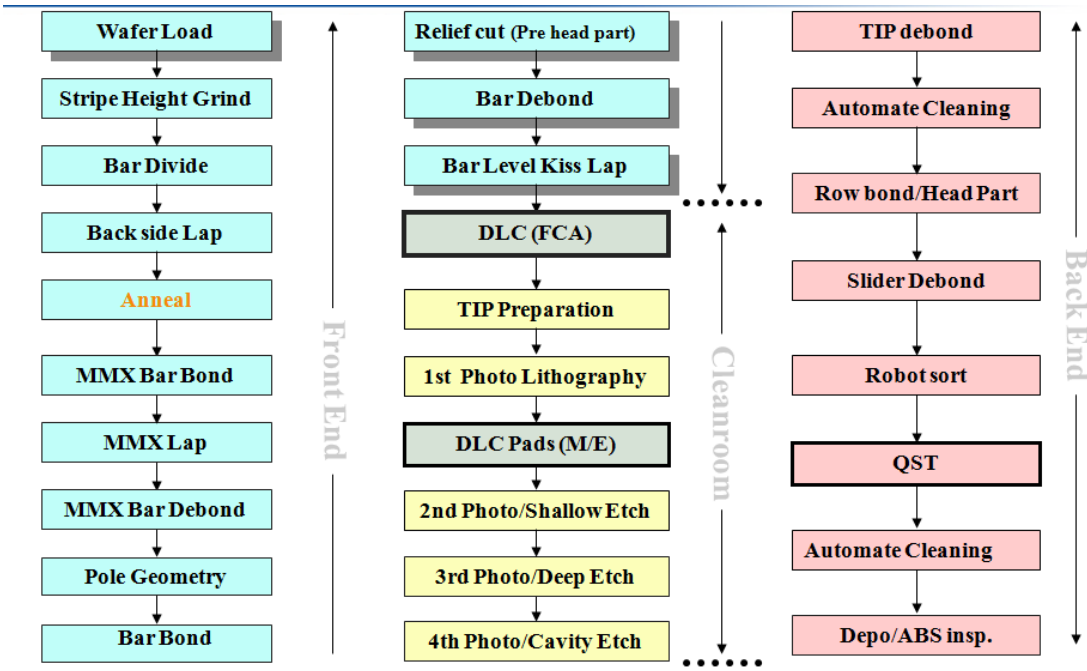

Fig. 3.2 Slider fab process flow

Fig. 3.3 and Fig. 3.4 show finished slider consist of writer or transducer coil and magnetic read sensor connected to bonding pad by very small lead line at deposition side. ABS surface consist of Landing pads, Landing Edge, Shallow Etch, Cavity Etch and Trailing Edge which are engineer to fly above the disk in nanometer scale.

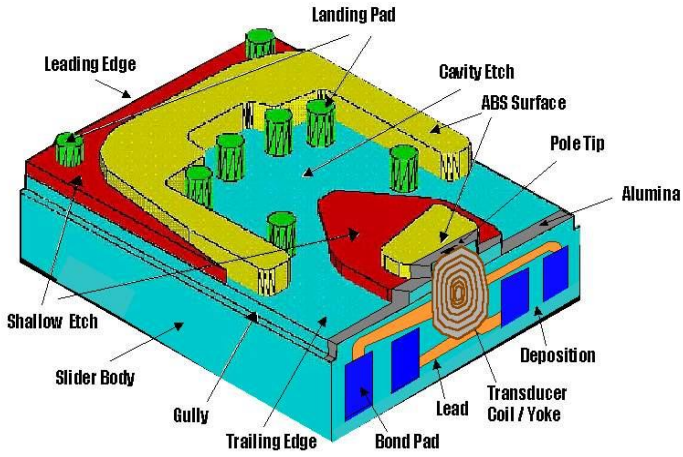

Fig. 3.3 Slider component

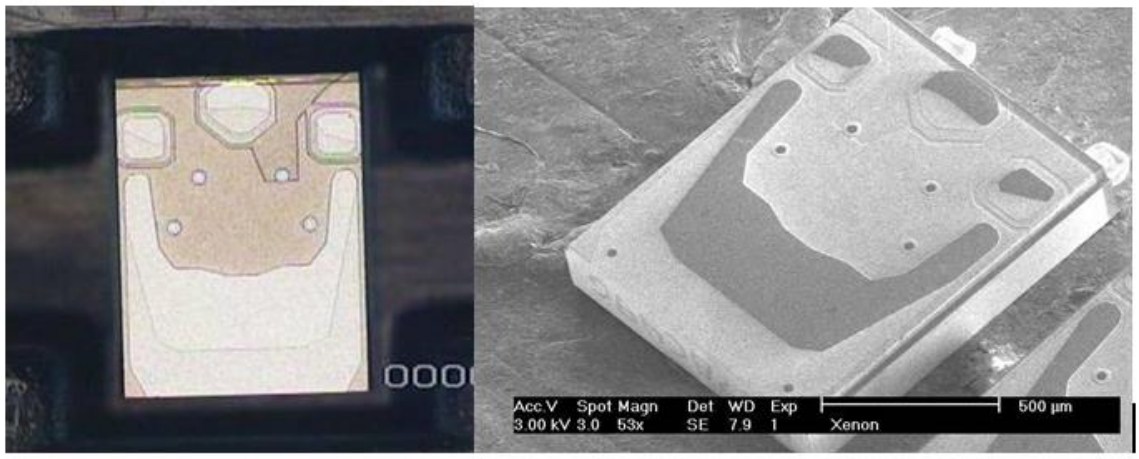

Fig. 3.4 Slider ABS side

3.2.2 Head Gimbal Assembly (HGA) process flow.

Concept of Head Gimbal Assembly (HGA) process is attaching slider with suspension. The process flow is shown in Fig. 3.5 and then HGA is shown in Fig.3.6. First step is loading from suspension from trays to in-process pallet and use epoxy application for bonding slider and suspension. After that use Infra-red curing (IR oven) to cure epoxy that bonds the slider and suspension. Then make the electrical connection between slider and suspension through soldering (SJB). Next perform inspection using Visual Mechanical Inspection (VMI) of HGAs with low power (10X) and high power (100X). Finally auto-unload HGAs from in-process pallets to HGA trays.

This completes the sample preparation and the sample is ready for blocking temperature (T_b) test with Quasi Static test (QST) machine.

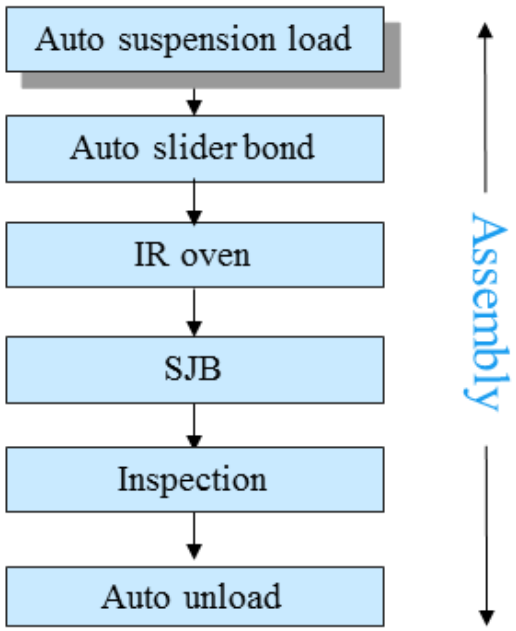

Fig. 3.5 Head Gimbal Assembly (HGA) process flow

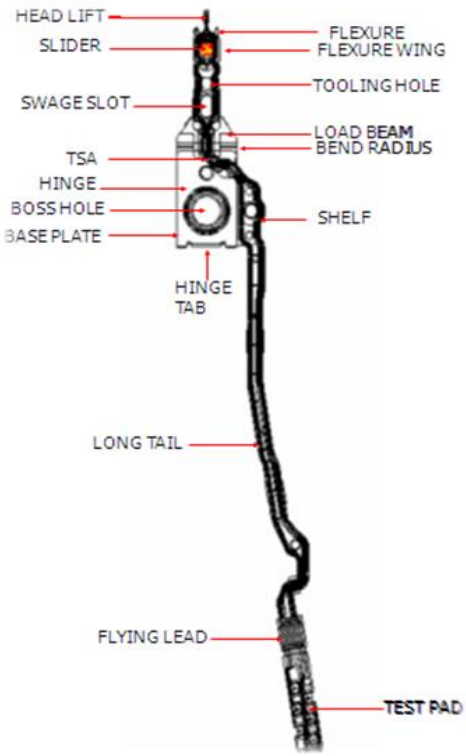

Fig. 3.6 Head Assemble Gimbal (HGA) overview

3.3 Quasi-Static tester at head gimbal assembly (HGA) form

The Quasi-Static Tester (QST) as illustrated in Fig. 3.7 is an engineering and production test system for characterizing the performance of magnetic read heads (MR). Unique mechanical configuration allows hard and easy transfer curves with a single magnet. The transverse (Hard) and longitudinal (Easy) transfer curve are acquired at constant bias current by measuring Amplitude across the read heads (MR) element while sweeping an applied magnetic field. The precision low-noise calibration circuitry allows maximum dynamic range for every measured point. From the transfer curve statistical results such as Amplitude, Asymmetry, and Barkhausen are automatically calculated along with Resistance and Bias Current during the test as shown in Fig. 3.8.

The Hard transfer curve can be used to quickly characterize the linearity of the magnetic read heads (MR) response to transverse magnetic field. The Easy axis transfer curve can be used to evaluate magnetic read heads (MR) element shields breakdown. Also, high longitudinal field can be applied to reset magnetic domains in the magnetic read heads (MR) element. For engineering analysis, the tester can perform the following tests while applying thermal, bias current, and write element excitation stresses to magnetic read heads (MR).

Quasi-Static Tester (QST) is ideal for head gimbal assembly (HGA) sampling, failure analysis, and production level head evaluation. The high magnetic field strength supports magnetic read heads (MR) domain polarization prior to testing. [11],[12],[13]

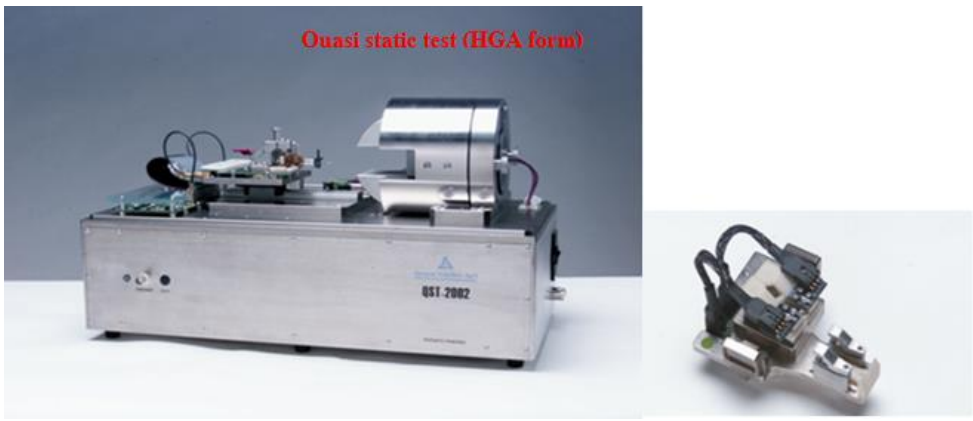

Fig. 3.7 Quasi-Static Tester at HGA level

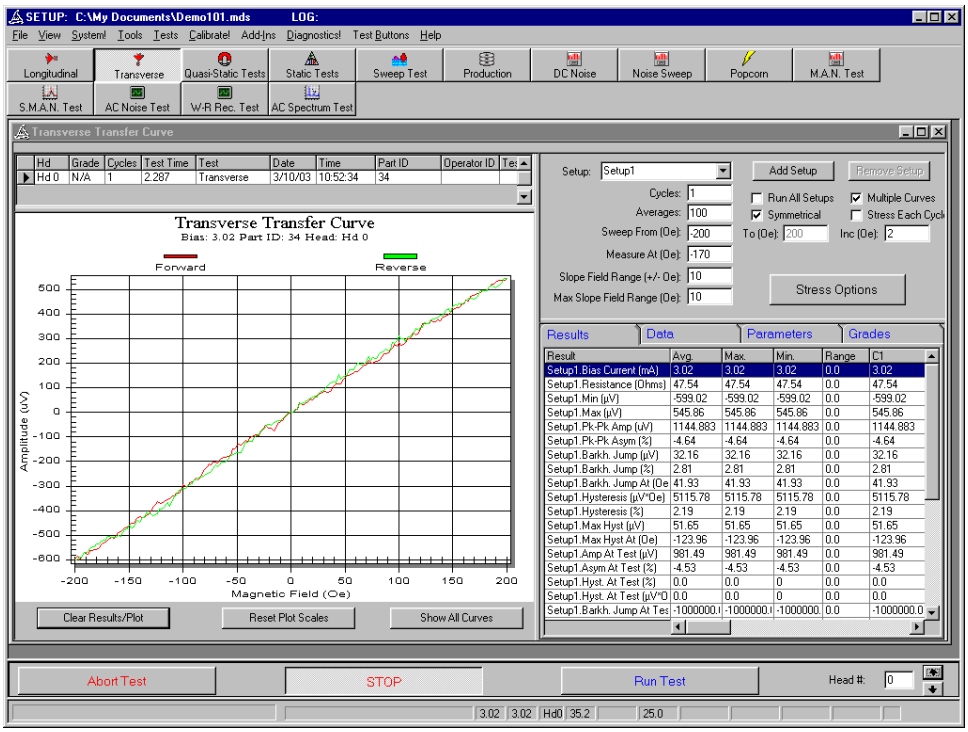

Fig. 3.8 Example of Transverse Transfer Curve from QST tester

3.3.1 QST parametric measurements

a) MR resistance

The MR resistance test is the basic MR production test. In theory, MR amplitude is proportional to the Magneto-Resistive Resistance (MRR) for small signals when a fixed bias current is used in testing. The MR resistance is calculated by measuring the sense element's voltage when a known bias current is circulating through the element as in Fig. 3.9.

MRR is define as

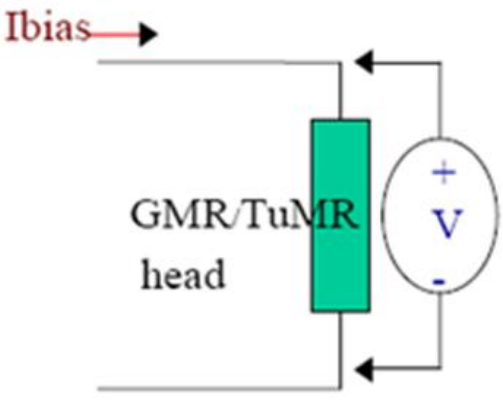

$$R_{MR} = \frac{V_{MR}}{I_{BIAS}}$$

Fig. 3.9 MRR measurement

b) MR transfer curve

The MR transfer curve measurement is essential in determining subtle head changes in magnetic performance. As shown in Fig. 3.10, the MR transfer curve can also reveal over-stressed heads that are suspected of being overlapped, which results in high resistance. High resistance results in the head temperature being too high under nominal bias current

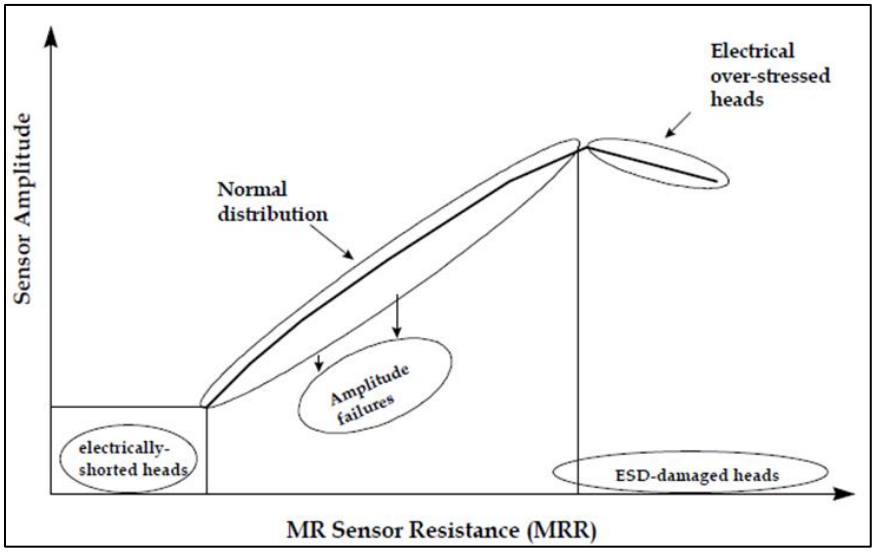

Fig. 3.10 MR amplitude and its relation with MR resistance

The resistance of a MR sensor is measured using a 4-point contact technique. MR bias current can be adjusted according to its resistance value to optimize its performance. Lower bias currents should be used for MR sensors with higher resistance or over-heating may occur which degrades the performance of the MR sensor. The resistance of a MR sensor is a linear function of the temperature. The increase in sensor temperature from the ambient is proportional to the total power dissipated which is a parabolic function of bias current as shown in Fig. 3.11.

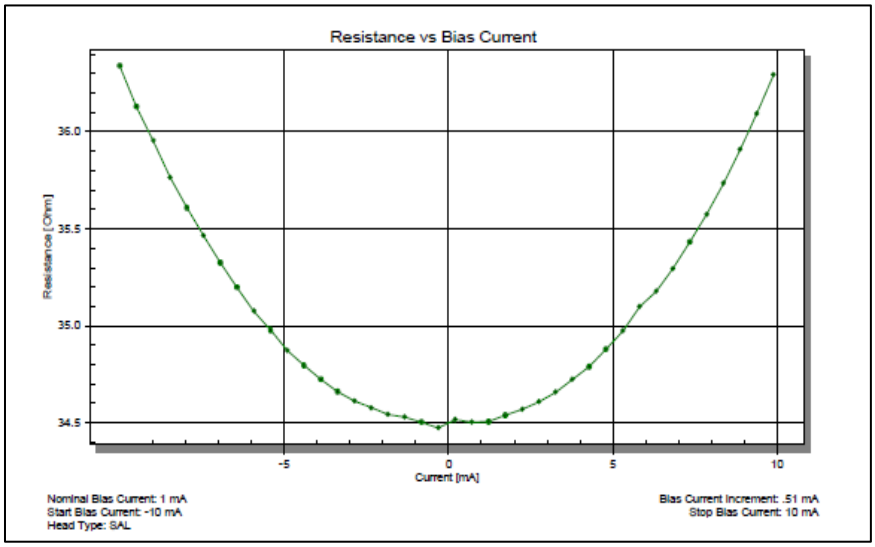

Fig. 3.11 MR resistance vs. bias current

3.3.2 MR transfer curve test

MR transfer curves can be readily obtained using a QST with a uniform external field applied to the sensor head. Amplitude, Asymmetry, Barkhausen noise and hysteresis can be extracted from the quasi-static transfer curve.

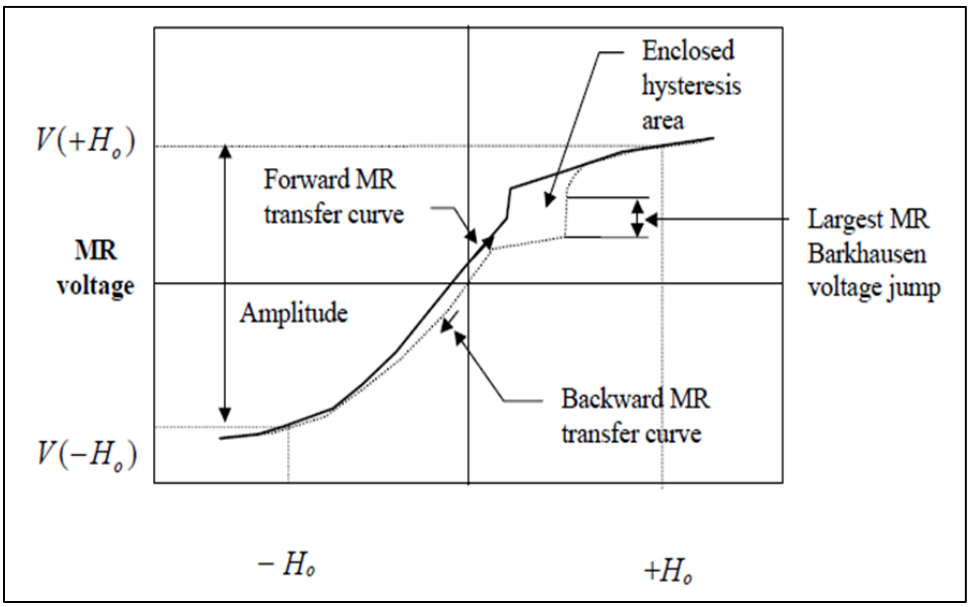

Fig. 3.12 Illustration of MR transfer curves and related measurements

Amplitude is defined as

$$Amplitude = V(+H_0) - V(-H_0)$$

Where $V(+H_0)$ is MR voltage at the specified external magnetic fields.

Asymmetry is defined as

$$Asymmetry = \frac{V(+H_0) - V(-H_0)}{V(+H_0) + V(-H_0)} \times 100\%$$

Hysteresis, as shown in Fig. 3.13 is defined as the absolute value of the difference between the area under the forward and reverse subsets of the transfer curve divided by the sum area of the forward and reverse curves, then multiplied by 100.

$$Hysteresis\_Percent = \left| \frac{AreaDifference}{AreaAverage} \right| * 100[\%]$$

Where the areas are defined with respect with the minimum amplitude and are calculated as

$$AreaDifferce = \sum_i \left(\frac{f_i + f_{i+1}}{2} - \frac{r_i + r_{i+1}}{2} \right) * \left(H_{i+1} - H_i \right)$$

and

$$AreaAverage = \sum_i \left| \frac{(f_1 + f_{i+1})/2 + (r_i + r_{i+1})/2}{2} \right| * (H_{i+1} - H_i)$$

The sign of the bias current is taken into account when determining the minimum (minimum “resistance” instead of the minimum voltage)

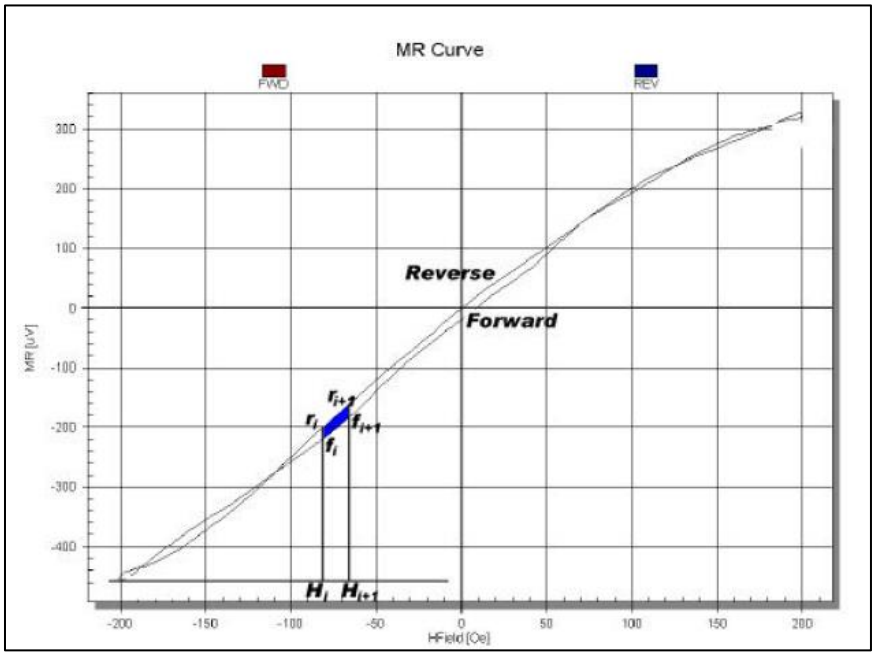

Fig. 3.13 Hysteresis represents the area between the forward and reverse curve

As shown in Fig. 3.14, Barkhausennoise characterizes the sudden jumps in the MR transfer curve. The result returns the value of the largest Barkhausen jump, expressed as a percentage, defined as the amplitude in [uV] of the largest point-to-point voltage jump within the specified number of cycles of the MR curve divided by the average peak to peak amplitude over the same number of cycles and multiplied by 100.

$$Barkhausennoise = 100 * LarestVoltageDelta / AverageAmplitude$$

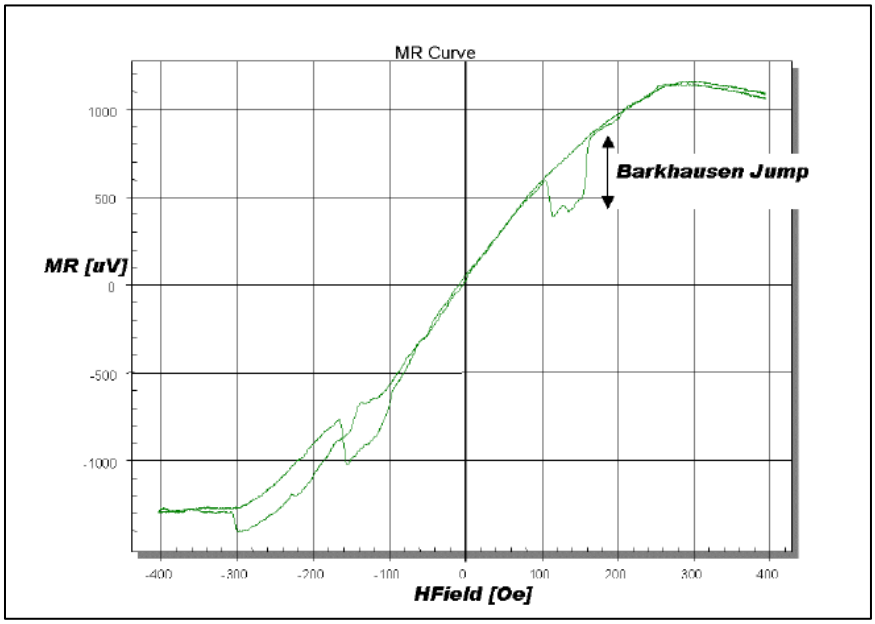

Fig. 3.14 The Barkhausen jump is actually calculated over all acquired cycles

The Sensitivity result measures the sensitivity of the device to a magnetic field and corresponds to the slope of the transfer curve, as shown in Fig. 3.15.

Slope is define as

$$Sensitivity = \frac{V(+H) - V(-H)}{(+H) - (-H)} * sign(BiasCurrent)$$

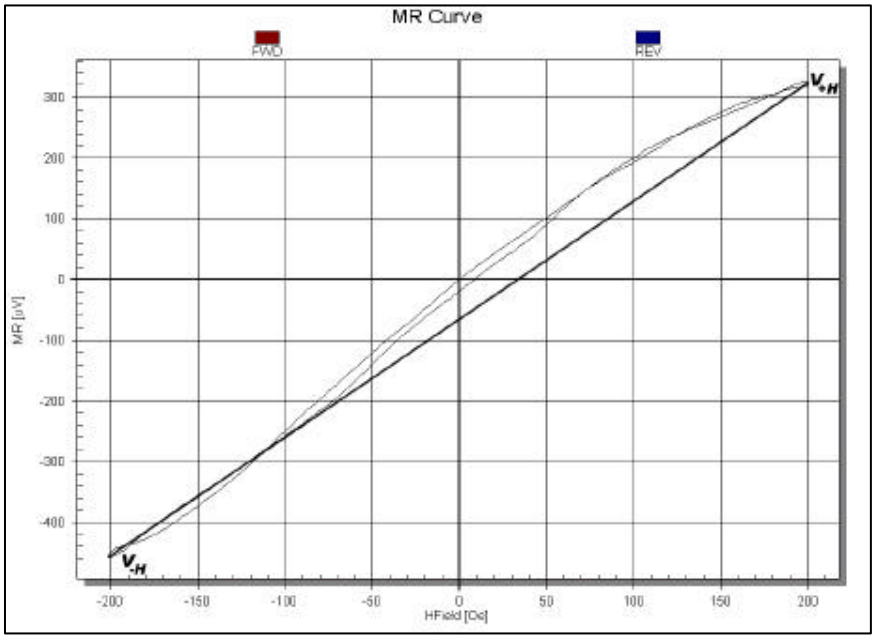

Fig. 3.15 The sensitivity or slope of the transfer curve (straight line)
Note: Sensitivity is independent from Asymmetry H Field Dependence

3.3.3 Spectral maximum amplitude noise test (SMAN)

SMAN test has been proven superior to conventional Transfer Curves at catching noisy or unstable heads. These heads normally exhibit soft kinks when using conventional Transfer Curves. Fast test time allows for use in Production to catch the same field instabilities. Initial Threshold can be used to further optimize the test. These phenomena have been linked to loosed of Bit Error Rate at Drive Level

SMAN test is designed to quickly measure the spectral noise density as a function of magnetic field utilizing AC channel and 160Mhz 10-bit digitizer. Optionally user can enable write stress to catch both writer induced and field induced noise.

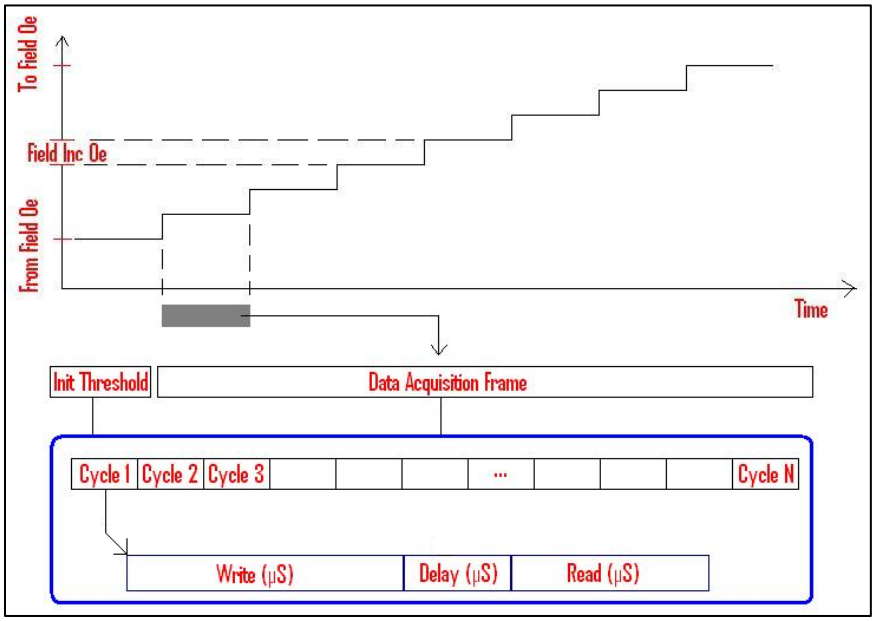

Fig. 3.16 SMAN Test Diagram

SMAN has 3 basic results, which are MaxNoiseAmp, NoiseAmp, and NoiseRMS. All these results come from digitizing ~250uS worth of data at each Field. At the end of the test software plots all 3 of these calculations performed at every Field value. For the 250uS of data at each field, this is not read in one large chunk, but actually is captured over several cycles. Each cycle size is defined by read length. Once the 250uS of data is read in, the calculations are performed as follows;

First, the MaxNoiseAmp is just the single highest noise spike read from this data.

Second, the NoiseRMS will be calculated, using all 250uS worth of data.

Third, the NoiseAmp calculation, will find the highest noise spike in each cycle. Then add up all of the highest noise spikes and divide by the number of cycles, ie get the average of the highest noise spikes. This result gives a combination of noise amplitude and probability. If there is a very high noise spike, but all the others are low, then MaxNoiseAmp will be high, but the averaged NoiseAmp will be low. Alternately, if there is a lot of noise, but none of these spikes are terribly high, then the NoiseAmp will be higher, and be very close to the MaxNoiseAmp.

At each field, if enabled, the tester runs initial threshold measurement before digitizing the noise. Initial Threshold simply sets user defined threshold and then runs the same sequence of write-delay-read cycles test, only counting the number of pulses that cross the threshold. If at least one pulse crosses the threshold, then the tester will proceed to Data Acquisition Frame. Initial threshold does not apply to the first and the

last field setting – at those field values the tester runs data acquisition frame to calculate noise metrics.

If initial threshold is enabled, naturally, measurements at some fields may be skipped. Such measurements will produce 0uV Noise Amp, Max Noise Amp and Noise RMS in raw data of the SMAN Result. Such measurements will not be included in statistical calculations of the SMAN test (Ave, Min, Max, and Range).

Noise RMS (μV)	Noise in μV (Root-Mean-Square value), calculated from digitized data from all read times.
Noise Amp (μV)	Average of the maximum noise amplitude seen in each cycle.
Max Noise Amp (μV)	Highest of the maximum noise amplitude seen ineach cycle.
Noise RMS-max Field (Oe)	Field that produces the highest Noise RMS value.
Noise Amp- Max Field (Oe)	Field that produce the highest Noise Amp value.
Max Noise Amp-Max Field (Oe)	Fied that produces the highest Max Noise Amp value.

Fig. 3.17 SMAN testing

In sum, three types of SMAN testing can indicated noise instability as follow

- NoiseRMS for broadband noise.
- MaxNoiseAmp for rare events such as barkhausen jumps and writer induced instability.
- NoiseAmp for high probability noise.

The SMAN test diagram, the SMAN testing parameters and the SMAN test result are shown in Fig. 3.16, Fig. 3.17 and Fig. 3.18 respectively.

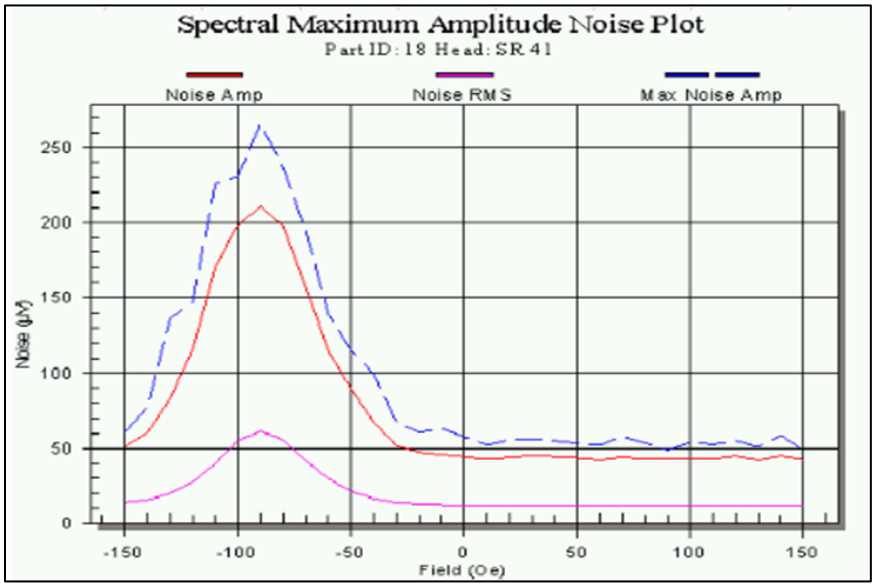

Fig. 3.18 SMAN result and printout

3.4 Blocking temperature measurement procedure

According to its pinning direction, the AFM layer can be reorient by annealing an FM/AFM system at a temperature is equal or more than the blocking temperature of the AFM layer. So, Blocking temperature (T_b) measurement procedure is as follow;

Step 1. Apply a high magnetic field to set the pinned layer (P1) in the direction opposite to the initial pinning direction, at the same time turn on DFH to heat the read sensor for a certain time, and then turn off the stress.

Step 2. After the stress, a high field transfer curve is measured, AFM pinning direction can be determined by the shape of the transfer curve.

Step 3. Keep increasing the DFH stress voltage and transfer curve measurement until the AFM pinning direction is reversed. Record the critical DFH stress voltage.

Transfer curves at different DFH stresses are shown in Fig. 3.19 (a) – Fig. 3.19 (f) respectively.

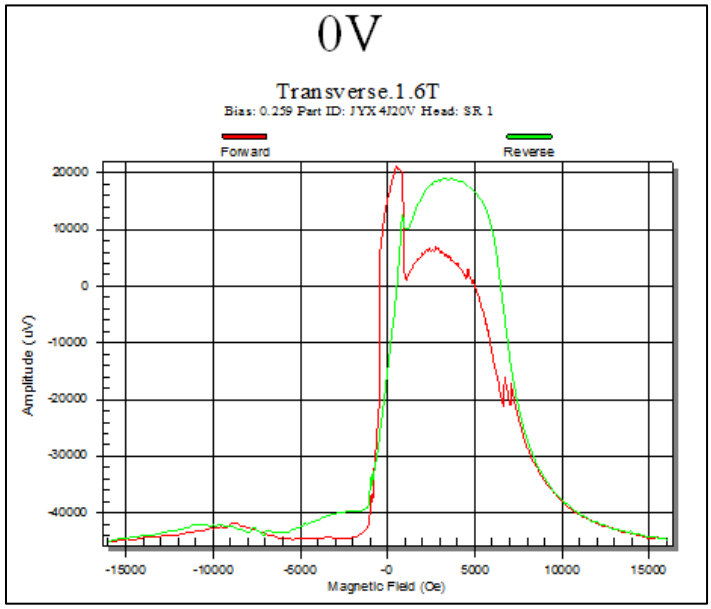

Fig. 3.19 (a) Tranfer curve at innitial state (DFH=0V).

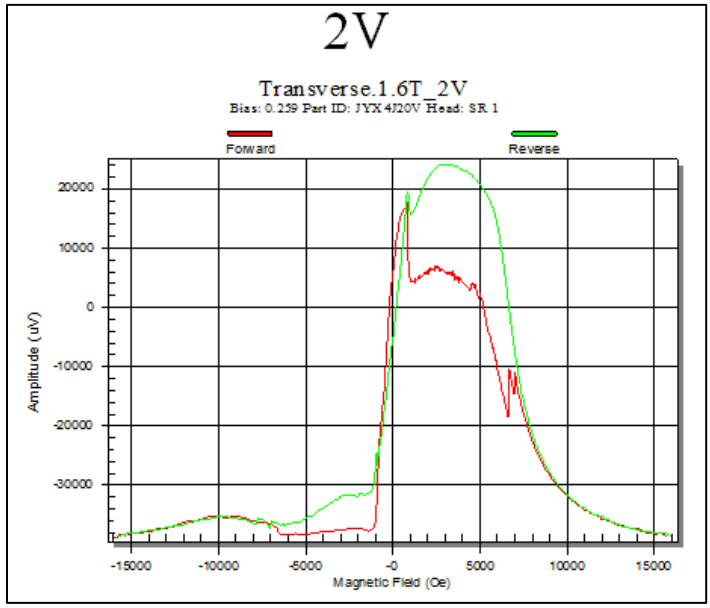

Fig. 3.19 (b) Tranfer curve at DFH=2V.

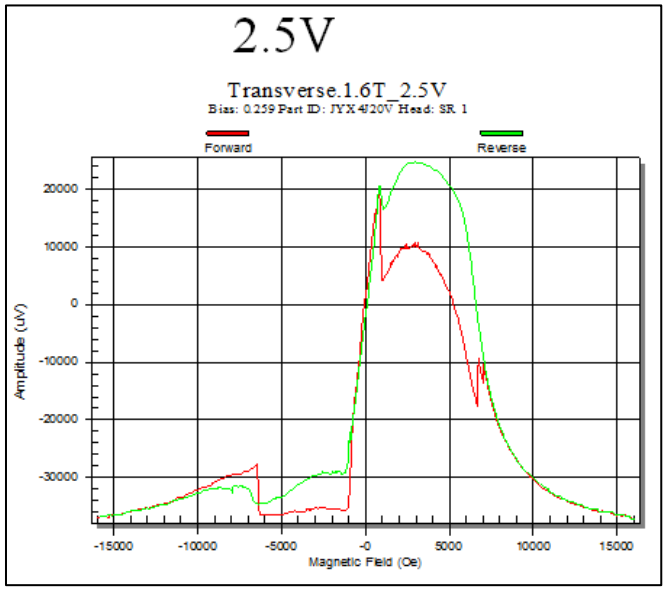

Fig. 3.19 (c) Tranfer curve at DFH=2.5V.

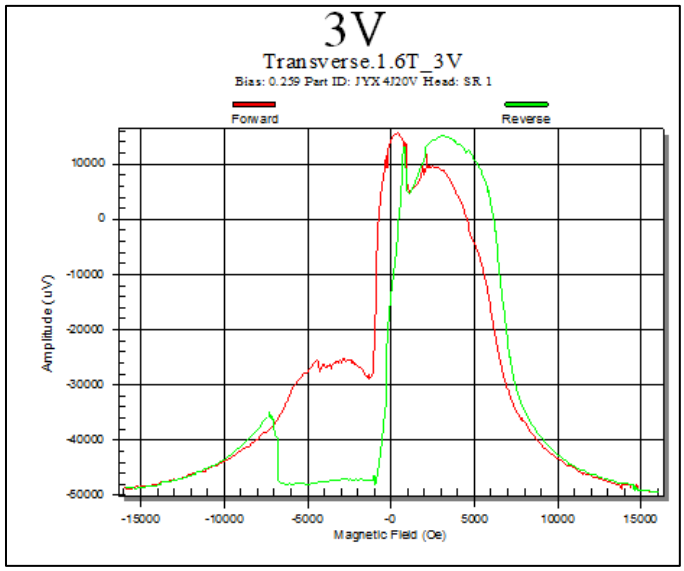

Fig. 3.19 (d) Tranfer curve at DFH=3V.

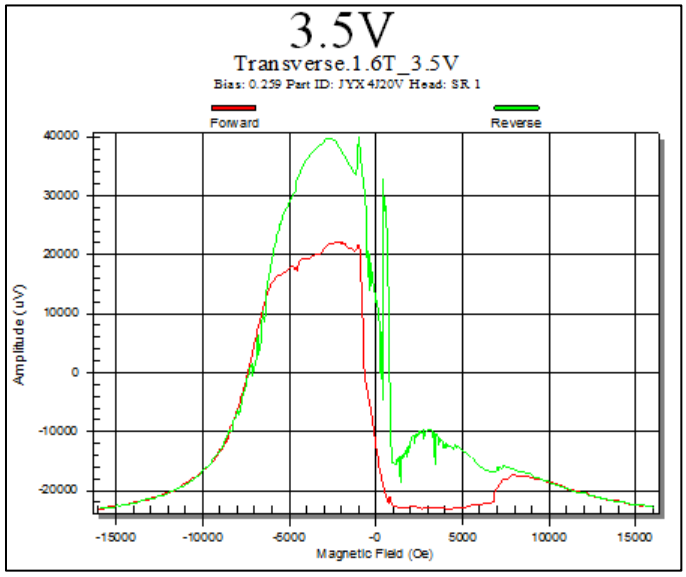

Fig. 3.19 (e) Transfer curve at DFH=3.5V.

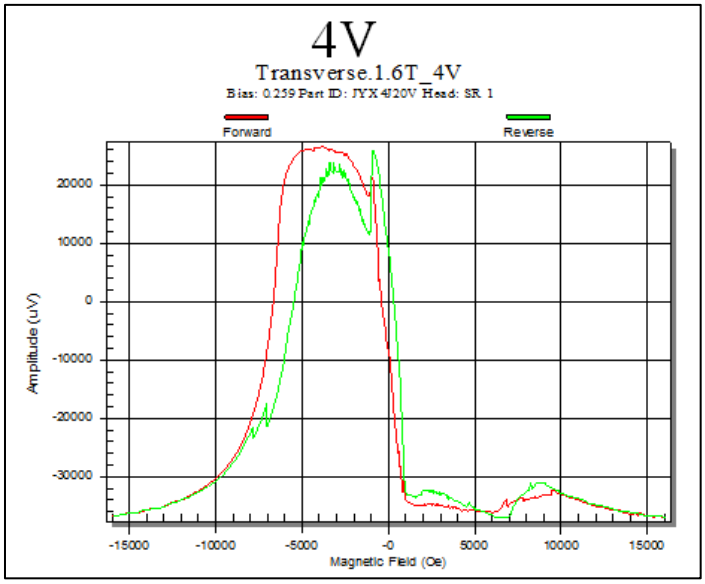

Fig. 3.19 (f) Transfer curve at DFH=4V.

Step 4. Zap the read sensor with a high stress current to make it a metallic sensor.

Step 5. Measure resistance vs. DFH voltage of the zapped read sensor, as shown in Fig. 3.19 (g).

- Measure the resistance of the zapped reader when DFH is turned on, and ramp the DFH voltage.

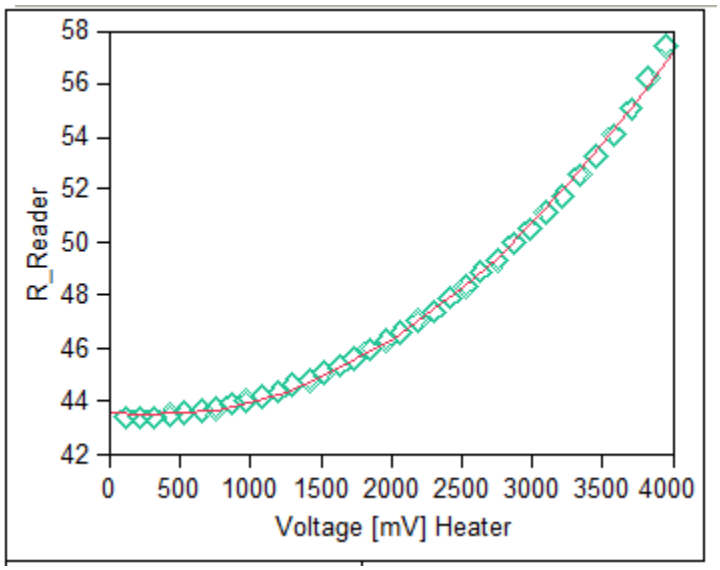

Fig. 3.19 (g) Resistance vs Voltage.

- Resistance should increase linearly with DFH power, $P = \frac{V^2}{R}$ where P is power, V is voltage and R is resistance. The plot of resistance vs Power is shown in Fig. 3.19 (h).

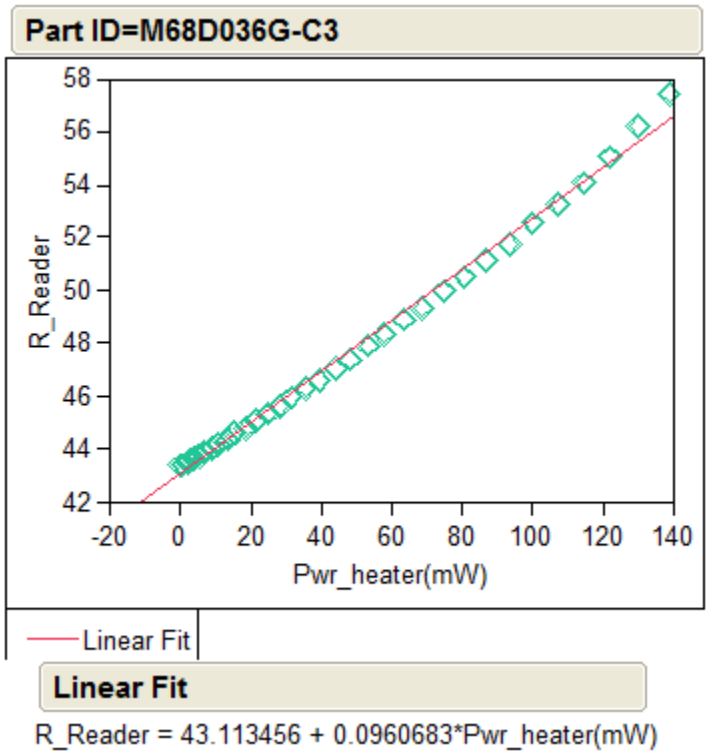

Fig. 3.19 (h) Resistance vs Power.

- Also need to measure DFH resistance vs DFH voltage, as shown in Fig. 3.19 (i).

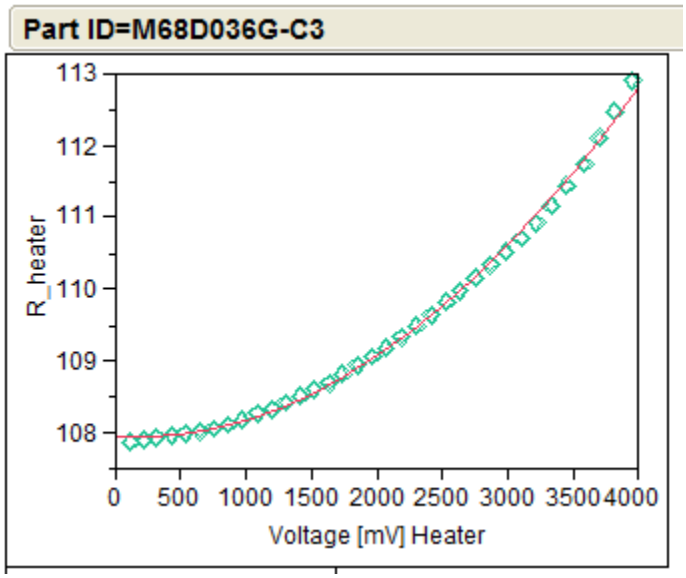

Fig. 3.19 (i) DFH resistance vs DFH voltage.

Step 6. Measure temperature vs. resistance of the zapped reader, as shown in Fig. 3.19 (j).

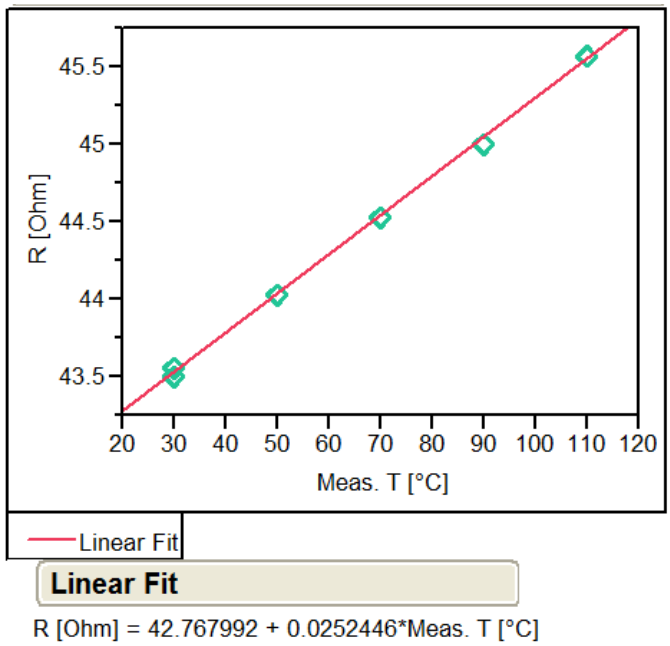

Fig. 3.19 (j) Resistance vs Temperature.

Step 7. Generate the correlation between read sensor temperature and DFH power from the above two measurements.

- Using equation from Fig 3.19 (h) and Fig 3.19 (j) to generate equation for finding the blocking temperature,

$$T_b = x + (y \times Power)$$ By x is constant value and y is slope.

Step 8. Calculate Blocking temperature (T_b) from the critical DFH voltage (power) and the temperature vs. DFH power correlation.

3.5 Transmission Electron Microscope (TEM)

Basic principle of Transmission Electron Microscope (TEM) is same as the light microscope but uses electrons instead of light and their much lower wavelength than light microscope. TEM is capable of imaging at a significantly higher resolution than light microscopes.

TEM is used for imaging of read sensor with high magnification and resolution at sub nanometer scale. The structure of the read sensor can be observed in transmission mode which is not possible with SEM. TEM and its components are shown in Fig. 3.20.

In this research TEM is used for measure the actual SH.

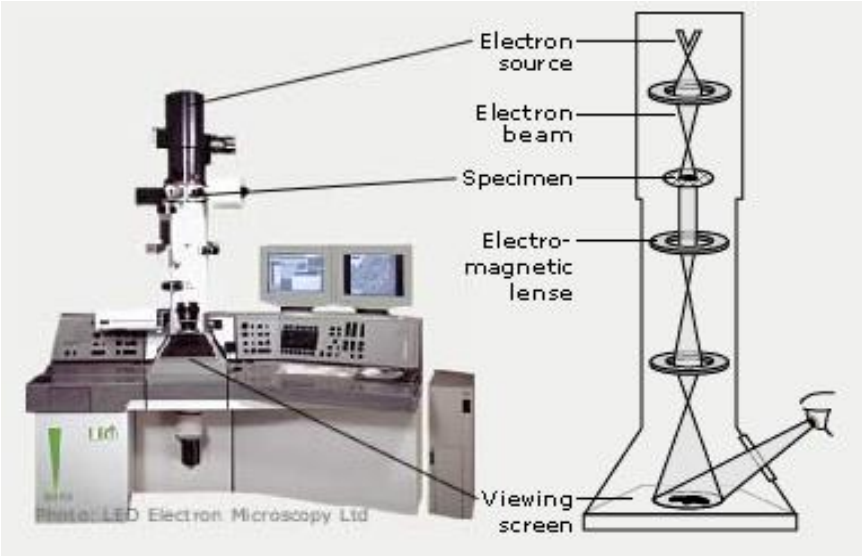

Fig. 3.20 Transmission Electron Microscope (TEM) [15]

3.6 Experiment plan

1. Study and review previous research about blocking temperature in magnetic read head.

2. Study blocking temperature test method by using ISI HGA machine at western digital's Bang pa-in.

3. Simulation blocking temperature value from equation 2.5 (Chapter 2) by vary RTW and SH (Using the same value as in experiment plan).

4.Preparation samples by using lapping machine and build up in HGA form.

a. Key design.
b. $1Tb/in^2$
c. Read track width (RTW).
d. Stripe height (SH).

5. Sample geometry is confirmed by electrical lapping guide data (ELG) and TEM measurement.

6. Test samples by Quasi Static test at HGA machine.

7. Analysis the data by using JMP program and Microsoft excel.

8. Conclusion and discussion.

Chapter 4
Result and Discussion

The experiment for this study and the data analysis are performed at Western Digital Bangpa-in plant and King Mongkut's Institute of Technology Ladkrabang. All experiments related to Tunnel magnetic resistance read head (TMR) system is performed on commercially available Quasi Static Tester (QST) and the statistical analysis is done using the statistical analysis tool "JMP" software.

There are two groups of samples, a group with 24 nm Read Track Width (RTW) and other group with 27 nm RTW. In each group, there are 5 different SH targets which are 12nm, 17nm, 27nm, 37nm, and 42 nm respectively.

4.1 Process results

This experiment used Electrical Lapping Guild resistance (ELG) in slider lapping process to control reader stripe height (SH). Individual TMR design has different correlation between ELG and SH. This TMR design has followed the standard mathematical equation from the design team at Bangpa-in plant.

$$SH = (Slope \times ELG) + Intercept$$

Equation above is a linear correlation between variables, ELG and SH. The SH which depends on magnetic material and sensitivity. Practically, in hard disk drive manufacturing, SH is targeted by ELG resistance in lapping process. Table 4.1 shows ELG resistance target at lapping process to define SH target. However current slider fabrication manufacturing process still has process deviation. Table 4.2 shows target ELG versus actual ELG for every SH on both RTW. Delta to target is about 1-5ohm within normal distribution.

RTW	Material	12nm	17nm	27nm	37nm	42nm
24nm	No 1	966.5	992.0	906.8	869.4	822.6
	No 2	978.9	1004.7	918.4	880.5	833.1
27nm	No 1	1006.5	924.2	975.7	871.4	828.5
	No 2	1018.1	934.9	987.1	881.5	838.1

Table 4.1 ELG resistance targets.

		24 RTW			27 RTW		
SH Group	Material	Target	Actual	delta (Actual - Target)	Target	Actual	delta (Actual - Target)
12nm	No 1	992.0	*993.4*	*1.4*	1006.5	*1011.4*	*4.9*
	No 2	1004.7	*1003.6*	*-1.1*	1018.1	*1013.3*	*-4.8*
17nm	No 1	966.5	*969.3*	*2.9*	975.7	*977.2*	*1.4*
	No 2	978.9	*977.8*	*-1.1*	987.1	*985.8*	*-1.2*
27nm	No 1	906.8	*915.5*	*8.6*	924.2	*930.4*	*6.2*
	No 2	918.4	*910.5*	*-8.0*	934.9	*929.9*	*-5.0*
37nm	No 1	869.4	*866.7*	*-2.6*	871.4	*874.7*	*3.3*
	No 2	880.5	*883.9*	*3.4*	881.5	*878.8*	*-2.7*
42nm	No 1	822.6	*826.3*	*3.7*	828.5	*832.1*	*3.6*
	No 2	833.1	*830.5*	*-2.7*	838.1	*834.7*	*-3.4*
		Average		1.4			4.9

Table 4.2 shows the target and actual ELG resistance.

Fig. 4.1 and Fig. 4.2 show the comparison between target and actual ELG resistance for both 24nm and 27nm RTW. The actuals are close to targets.

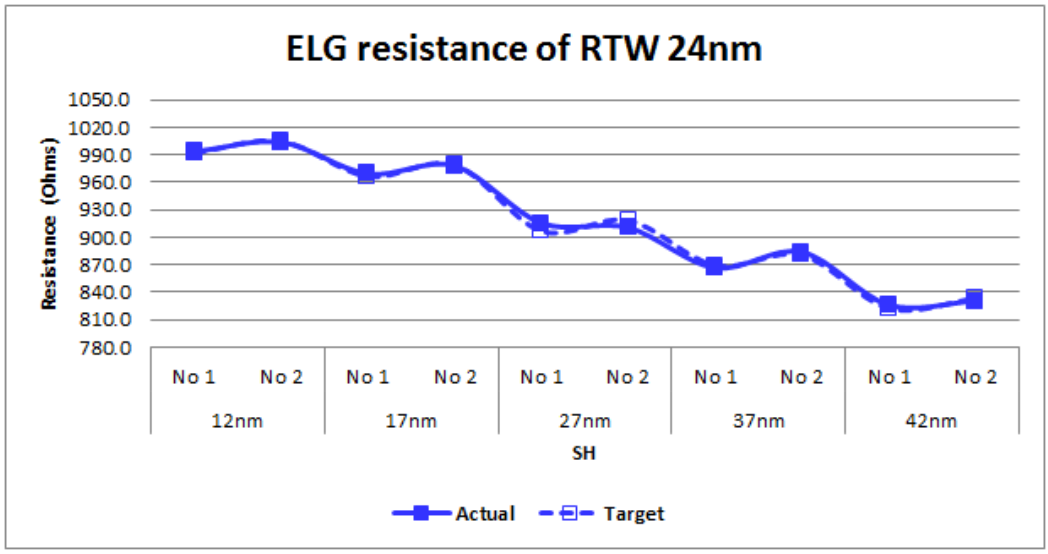

Fig. 4.1 ELG resistance target vs actual of RTW 24nm.

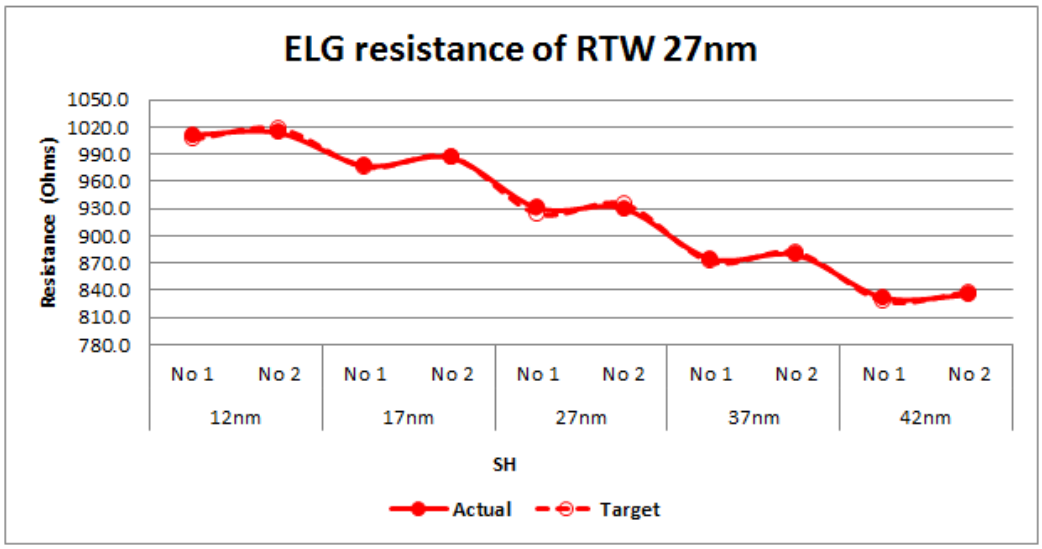

Fig. 4.2 ELG resistance target vs actual of RTW 27nm.

All 24nm and 27nm RTW targets were validated to physical SH using cross section TEM. Fig. 4.3 shows TEM pictures of samples cross section with different SH targets for RTW 24nm. This proves that we can achieve physical SH as expected.

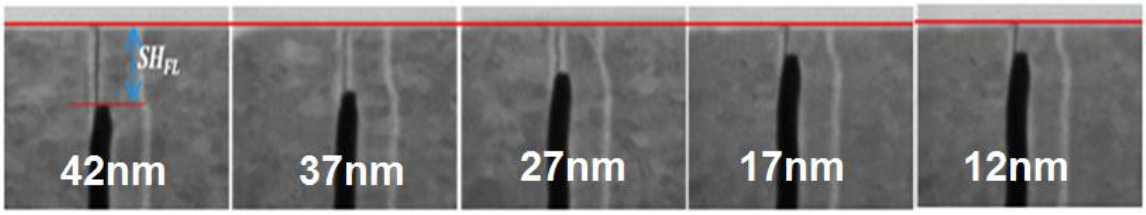

Fig. 4.3 Cross section TEM image different SH

4.2 Experiment results

Table 4.3 shows the result from blocking temperature testing. It shows Resistance, Amplitude, Power, Blocking temperature and Static Signal to Noise ratio (SNR) of each SH. These parameters are measured by Quasi Static tester in order to find the correlation between blocking temperature and stripe height.

Resistances strongly track to SH. Samples with longer SH have a lower resistance for both RTW 24nm and 27nm. Blocking temp is also impacted from SH. Samples longer SH have a higher blocking temperature both RTW. Finally, for the Static Signal to Noise ratio, the most important parameters for Hard disk drive performances, the longer SH results in better Signal to Noise ratio.

SH target		12nm	17nm	27nm	37nm	42nm
RTW 24nm	Resistance (Ohms)	848	748	583	481	425
	Amplitude (uV)	13342.1	12168.7	11990.4	11642.4	9942.3
	Power (mW)	68.9	71.4	71.9	71.8	71.7
	Tb (°C)	281.3	290.6	292.4	292.0	291.8
	SNR (dB)	23.5	23.5	25.1	25.9	26.2
RTW 27nm	Resistance (Ohms)	849	705	532	405	328
	Amplitude (uV)	14941.9	16217.6	17211.4	15001.6	14165.9
	Power (mW)	71.1	70.7	73.4	75.6	78.8
	Tb(°C)	288.0	296.8	302.8	310.0	317.8
	SNR (dB)	24.4	25.4	28.3	29.7	29.5

Table 4.3 Table summary of Experiment results

4.2.1 Resistance by various SH

Fig. 4.4 is a plot of measured resistance at various SH. It shows that the resistance decreases as the SH increases. This chart explains that increasing resistances with decreasing SH for both RTWs. As expected, small magnetic read area will results in high resistance. Therefor SH variation in actual manufacturing can be monitored by using resistance measurement.

More analysis will be shown here in Fig. 4.4, which is shown the relation between SH and Resistance. The resistance is high when SH is short; both of RTW design are showing the same trend. The Resistance and SH strongly correlated in inversely, which is follow the expectation. Reader volume reduced from short SH impact to higher resistance. On the other hand we can review the reader volume by RTW analysis. RTW also impacts to resistance. At the same SH, the wider RTW 27nm show less resistance when compared to narrow RTW 24nm. Especially at the longer SH can see differentiate clearly.

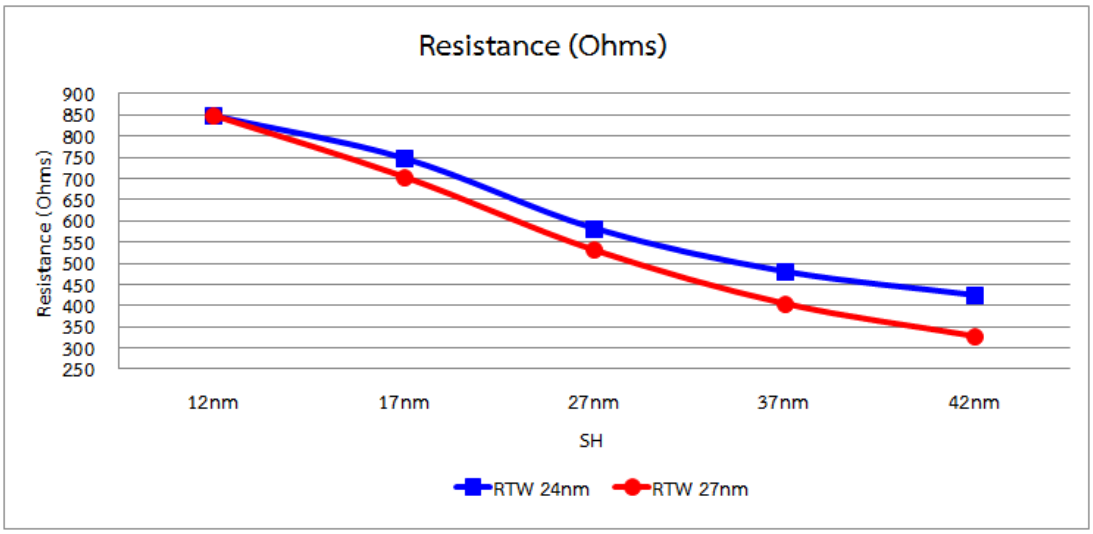

Fig. 4.4 Resistance by various SH

However in order to optimize magnetic reading head by SH and RTW, it needs to study other key parameters not only the resistance. Resistance however, is the most easily detectable parameters for reader volume change and correlates very well with reader SH and RTW when using quasi static tester.

4.2.2 Blocking temperature (T_b) by various SH

Base on equation 2.5 from Chapter 2,

$$T_b = \frac{K}{k_B \ln\left(\frac{\tau_m}{\tau_0}\right)} \cdot D^2 \frac{1}{1+\left(\frac{1}{a}+\frac{1}{b}\right)D}$$

This equation is used to estimate the blocking temperature value when RTW and SH are changed. The simulation results show in Table 4.4.

SH	RTW 24nm	RTW 27nm
	Tb (°C)	Tb(°C)
12nm	225.4	231.9
17nm	263.1	271.3
27nm	305.3	315.6
37nm	328.3	339.9
42nm	336.3	348.4

Table 4.4 Blocking temperature (°C) simulation

Fig. 4.5 shows simulation results of blocking temperature result for both RTW designs. Wider RTW (27nm) gives higher blocking temperature for every SH than narrower RTW (24nm).

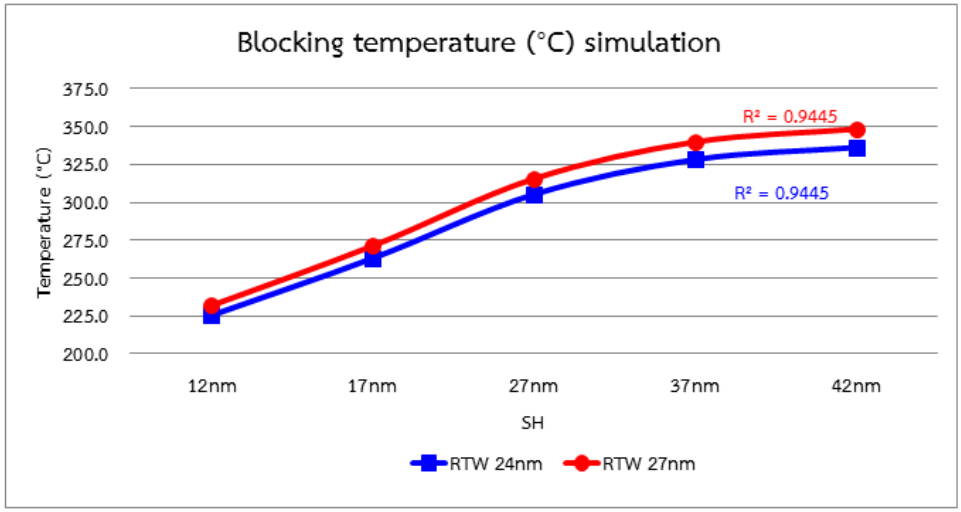

Fig. 4.5 Simulation results of blocking temperature (°C)

Fig. 4.6 shows the experiment result of blocking temperature with 2 RTW designs. For 27nm RTW, it increases with SH. The blocking temperature of the shortest SH and the longest SH is significantly lower and higher than that of the nominal SH. For 24nm RTW, only the blocking temperature at the shortest SH is significant by lower than that at the nominal SH. It is comparable for the longer ones. When SH is shorter than nominal SH only 10nm (approximately about 200Ohms resistance), blocking temperature decrease by 6°C. Therefor it can be used to detect reliability issue especially blocking temperature problem by defining the suitable resistance screening specification.

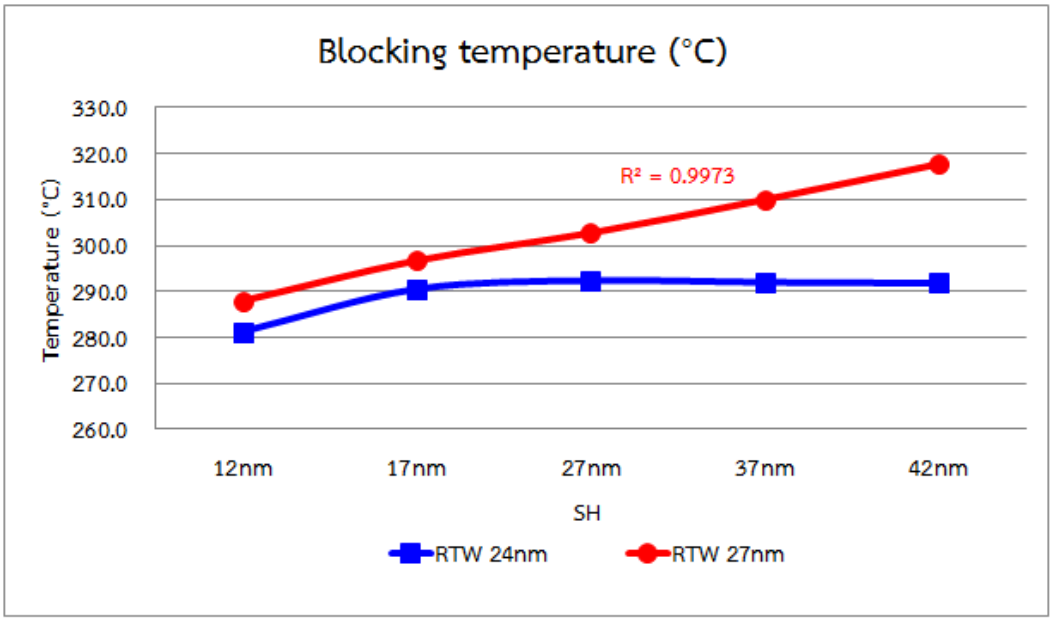

Fig. 4.6 blocking temperature (T_b) by various SH

SH also impacts to Blocking temperature. Fig. 4.6 shows a strong correlation (R-square) between SH and Blocking for both RTW 24nm and 27nm. R-square is the transfer function between factors (SH) to respond (temperature). With high R-square is reliable to expand the relation between factors to respond. Therefore, from this study, R-square is higher than 90% on 27nm RTW design. It is more confident that the SH is more effected to blocking temperature.

When compare between two designs, the wider 27nm RTW has potential better Blocking temperature with long SH while the narrower 24nm RTW has saturated Blocking temperature even with long SH. This can interpreted that blocking temperature depends on both SH and RTW, or the whole reader volume.

According to this result, blocking temperature can be by not reduce SH and RTW below a certain limit. Others improvement may need to studied due to this constraints.

However simulated values of blocking temperature are higher than experiment result on both RTW. Especially for 24nm RTW different behavior is the experiment result show saturated blocking temperature at long SH while the results simulation show increasing trend. This phenomenon may come from actual process variation. Ideally blocking temperature from simulation can be improved with further understanding and more investigation.

4.2.3 Blocking temperature vs Resistance

From above results, the relation between SH and resistance, SH and blocking temperature were observed. Then the relation between blocking temperature and resistance need to be verified.

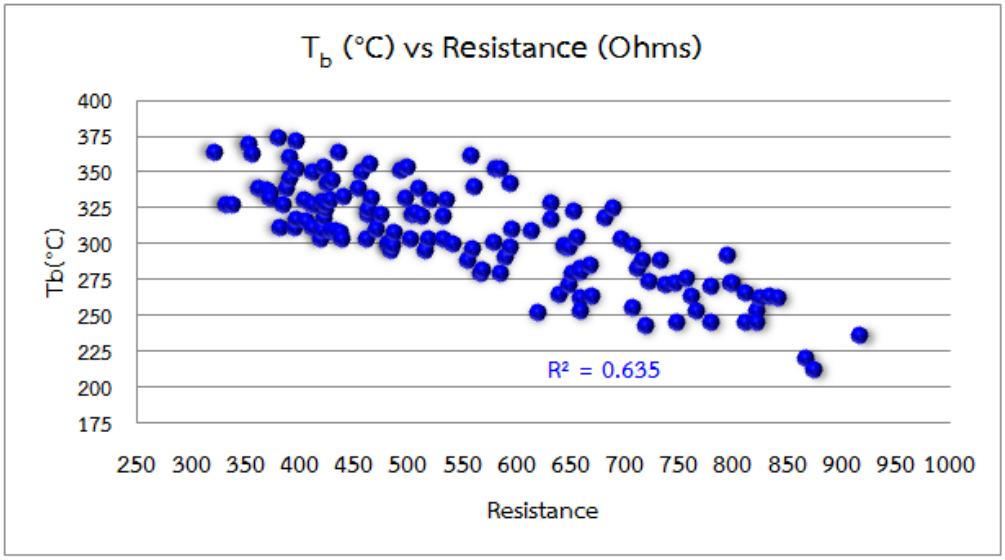

Fig. 4.7 Relation of T_b and Resistance

The relation of T_b and Resistance is shown in Fig. 4.7 the blocking temperature correlates to resistance value by 63% R-square. This result suggests us to use resistance for screening low blocking temperature which makes the reliability issue.

4.2.4 Signal to noise ratio (SNR) by various SH

Fig. 4.8 shows a plot of the signal to noise ratio (SNR) with different SH targets. The results show SNR trend to decrease with shorter SH target. Low SNR at short SH means high noise. Then noise is related to SH target.

Signal to noise ratio (SNR) is an important performance for hard disk drive technology. Higher areal density tends to have lower SNR. Blocking temperature and SNR are very important for magnetic reader performances. Fig. 4.8 shows a correlation between SH and SNR for both 24nm and 27nm RTW. Longer SH samples have better SNR for both RTWs. At same SH, wider RTW has better SNR. Moreover when SH is reduced to very narrow, both RTW show same SNR.

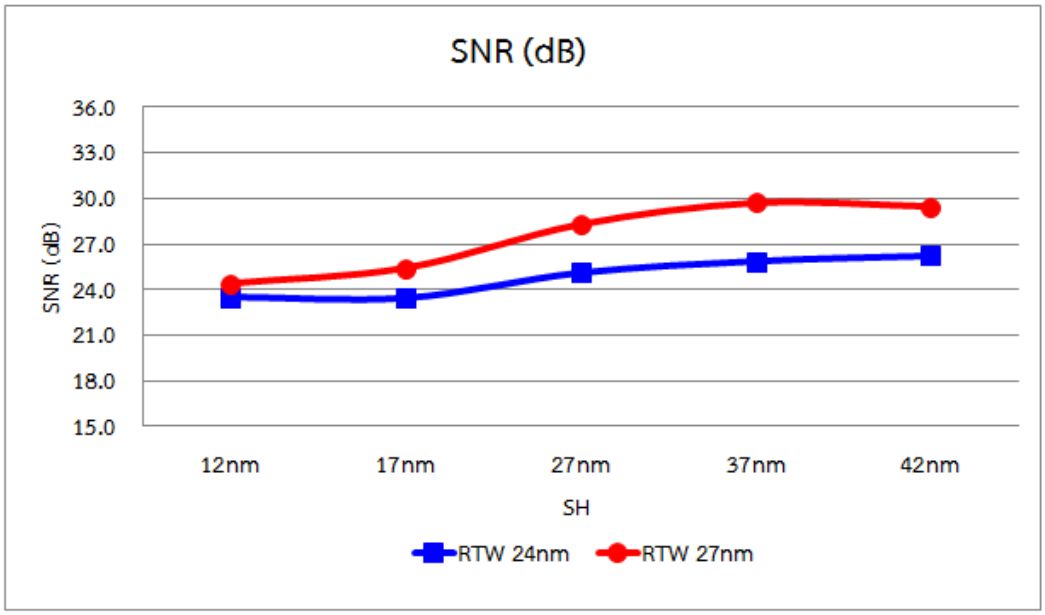

Fig. 4.8 SNR by various SH

4.2.5 Blocking temperature Tb (°C) by SH target and SNR

According to the correlation between Blocking temperature and Stripe height, has same impact as SNR which performs better at longer SH. SNR is very important performance in HDD manufacturing. Therefore, further analysis between SNR and Blocking temperature is necessary.

Fig. 4.9 shows a correlation between blocking temperature and SH, at different SNR. Blocking temperature and SNR have an increasing trend with longer SH however SNR and Blocking temperature show no clear correlation. So from these available experiment results it can be concluded that Blocking temperature and SNR not correlated. Blocking temperature and SNR can be improved by making SH longer.

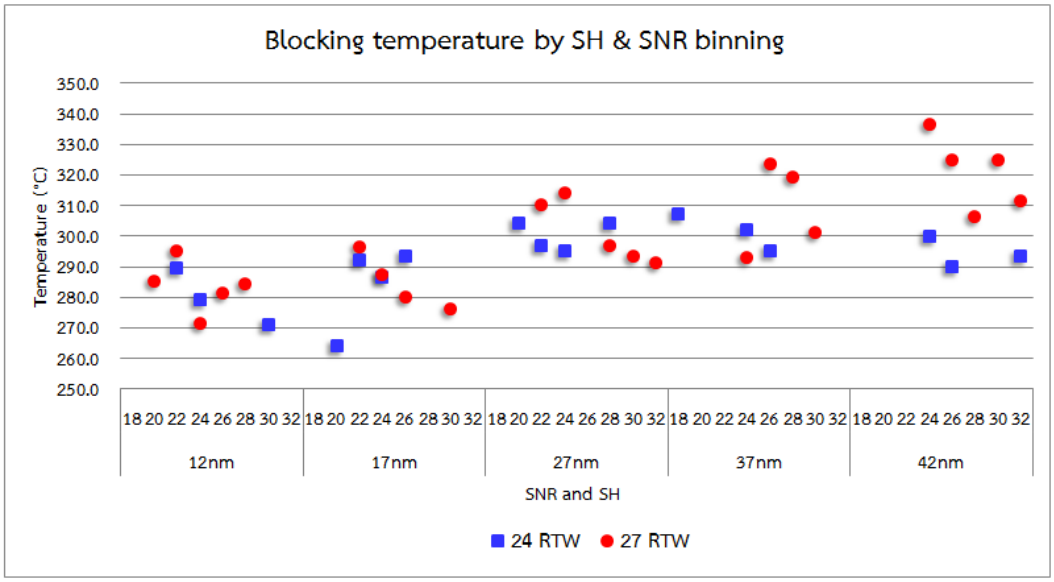

Fig. 4.9 blocking temperature (°C) by SH targets & SNR

4.2.6 Blocking temperature by reader area (RTW X SH)

Read track width (RTW) and Stripe height (SH) are focused for this study. These two dimensions are used as the reference reader area. Fig. 4.10 shows blocking temperature versus reader area. T_b is increases when reader area increases. However for 24nm RTW design, T_b is relatively constant where area is larger than 500nm^2.

From this result it shows that blocking temperature depends on reader area.

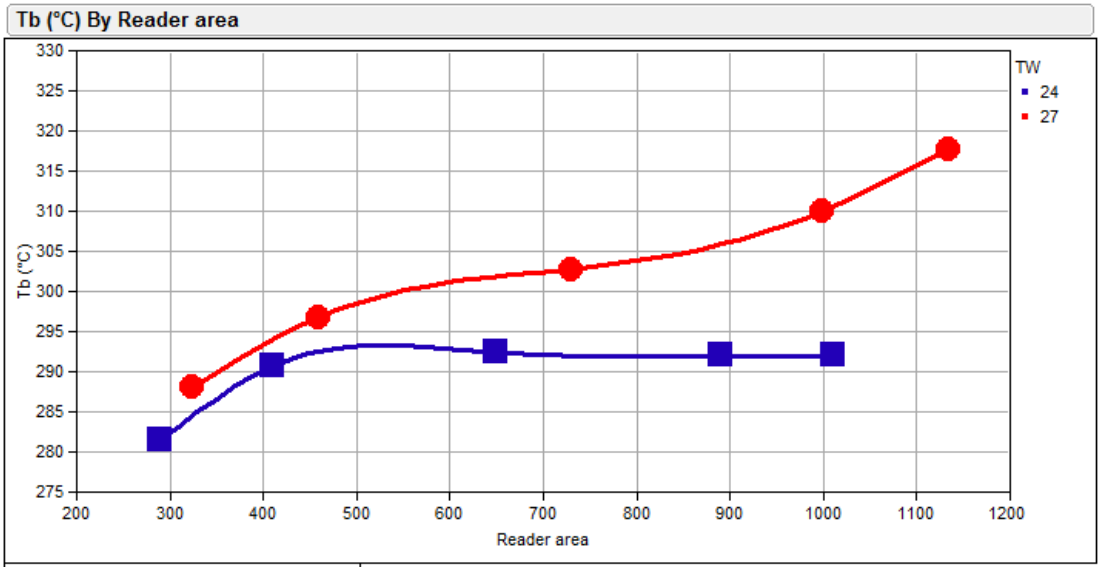

Fig. 4.10 blocking temperature (°C) by reader area (RTW X SH)

Chapter 5
Conclusion and Recommendation

5.1 Conclusion

The purpose of this study is to explore the magnetic read sensor performance using blocking temperature. Blocking temperature depends on reader volume, which also depends on the different in SH and RTW. In our experiment, there are 2 RTWs i.e. 24nm and 27nm. The short SHs achieve high resistance with lower blocking temperature for both RTWs. For long SHs, it shows different way. It gives low resistance with high blocking temperature only for the 27nm RTW. It is expected that the magnetic read performance is improved with higher blocking temperature. So from this study, it indicates that long SH is preferable. However areal density road map grows up with every dimensions shrink down. In fact, the need of magnetic read sensor to be small introduces some risks especially, lowering blocking temperature which will impact the reliability. To improve the magnetic read sensor performance in manufacturing, slightly long SH were considered. But this may not true for all cases, due to another RTW, the narrow 24nm, shows low blocking temperature on short SH but it does not increase even longer SH. This means that the blocking temperature cannot improve with the limitation of RTW. If RTW is too small, increasing SH will not increase the blocking temperature.

From the result of varying SH, using QST for electrical performance and TEM cross section for physical validation, the observed resistance and SH show a reverse trend based on current manufacturing process can achieved SH as expectation. So to confirm sample quality before continue to do Blocking temperature is important for this study due to manufacturing process may have some deviation.

For blocking temperature testing, 27nm RTW shows high blocking temperature with long SH target and low blocking temperature with short SH. 24nm RTW shows low blocking temperature with short SH same as RTW 27nm but blocking temperature maintain with long SH. So in HDD technology with higher areal density growth situation can be improved blocking temperature by maintain SH and RTW.

Signal to noise ratio (SNR) is an important parameter for hard disk drive. The correlation between SNR and SH shows similar trend as blocking temperature. At short SH SNR is less than at long SH for both 24nm and 27nm RTW. From this study with

available RTW, 27nm RTW has better SNR for all SHs. However no correlations observed between SNR and blocking temperature

5.2 Recommendation

Stripe height and read track width are not only key factors for blocking temperature improvement, other factors such as pinned layer, AFM thickness and composition are also important. Further study need to be carried out to gain more understanding and improvement in read performance.

References

[1] Y. Chen, D. Song, J. Qiu, P. Kolbo, L. Wang, Q. He, M. Covington, S. Stokes, V. Sapozhnikov, D. Dimitrov, K. Gao, and B. Miller, **"2 Tb/in2 Reader Design Outlook"**, Magnetics, IEEE Transactions on, vol. 46, pp. 697-701.

[2] Jeffrey R. Childress, Robert E. Fontana Jr, **"Magnetic recording read head sensor technology"**, C. R. Physique 6 (2005) 997–1012.

[3] Morgan Madec, Jean-Baptiste Kammerer, and Luc Hébrard, **"Compact Modeling of a Magnetic Tunnel Junction—Part II: Tunneling Current Model"**, IEEE, Vol. 57, No. 6, June 2010.

[4] Jian-Gang (Jimmy) Zhu, and Chando Park, **"Magnetic tunnel junctions"**, Western Digital Corporation, ISSN: 1369 7021, Elsevier Ltd 2006, Vol. 9, No. 11, Nov 2006.

[5] J. P.Nozie`res, S. Jaren, Y. B. Zhang, K. Pentek, A. Zeltser, P. Wills, and V. S. Speriosu , **"Correlation between lifetime and blocking temperature distribution in spin-valve structures"**, JOURNAL OF APPLIED PHYSICS, May 2000.

[6] Device physic, **"TuMR Reader Reliability"**, Western Digital Corporation, Fremont CA, 2013.

[7] L. Lombard, E. Gapihan, R. C. Sousa, Y. Dahmane, Y. Conraux, C. Portemont, C. Ducruet, Papusoi, I. L. Prejbeanu, J. P. Nozières,B. Dieny, and A. Schuhl, **"IrMn and FeMn blocking temperature dependence on heating pulse width"**, Journal of applied physics, 107, 09D728, 2010.

[8] Haiwen Xia and Robert M. White and Zheng Gao and Sining Mao, **"Antiferromagnetic thickness dependence of blocking temperature in exchange coupled polycrystalline Ferromagnet / Antiferromagnet bilayers"**, Journal of applied physics, Oct 2002.

[9] G. Vallejo-Fernandez, B. Kaeswurm, L. E. Fernandez-Outon, and K. O'Grady, **"Effect of the Ferromagnetic Layer Thickness on the Blocking Temperature in IrMn/CoFe Exchange Couples"**, IEEE transaction magnetics, Vol.44, No.11, Nov 2008.

[10] A. J. Devasahayama and M. H. Kryder, **“The dependence of the antiferromagnet/ferromagnet blocking temperature on antiferromagnet thickness and deposition conditions”**, Journal of applied physics, Apr 1999.

[11] Henry Patland, and Wade Ogle, **“Quasi Static Testing”**, 2192 Bering DriveSan Jose, CA 95131, Integral Solutions Int’l, www.isiguys.com.

[12] MRS200 Operation Manual, **“Quasi static Slider-Level Tester”**, Phase Metrics, San Diego Head Products Division, 2000.

[13] Integral Solutions Int’l, **“QST External Tests User’s Manual”**, 3000 Olcott St. Santa Clara, CA 95054, October 2011.

[14] N.Smith, **"Micromagnetic modeling of magnoise in magnetoresistive read sensors"**, Journal of Magnetism and Magnetoc Materials, vol. 321, pp. 531-538, 2009.

[15] http://www.nobelprize.org/educational/physics/microscopes/tem/index.html, The Transmission Electron Microscope.

[16] Manuel Benz, **“Superparamagnetism : Theory and Applications”**, Discussion of Two Papers on Magnetic Nanoparticles, December 14, 2012.

[17] Y. Ding, and C. Elliott, **“Simulation of grain size and blocking temperature in small devices”**, 15 November 2010.

Electrical Engineering Academic Association (Thailand)

The 2015 International Electrical Engineering Congress

The 2015 International Electrical Engineering Congress

(*i*EECON2015)

This certificate is presented to

CHAYAPIM KOLPROMSARO

For recognition of presenting a paper in the conference

Study the Effect of Strip Height and Read Track Width on Blocking Temperature

During March 18-20, 2015, Phuket City, Thailand

Professor Dr. Apirat Siritaratiwat

*i*EECON2015 General Chair

Applied Mechanics and Materials Vol. 781 (2015) pp 199-202
© (2015) Trans Tech Publications, Switzerland
doi:10.4028/www.scientific.net/AMM.781.199

Submitted: 2014-10-13
Revised: 2015-03-30
Accepted: 2015-04-06

Study the Effect of Stripe Height and Read Track Width on Blocking Temperature

C. Kulpromsaro[1,a] , K.Vichienchom [2,b] and W. Pijitrojana[3,c]

College of Data Storage Innovation

King Mongkut's Institute of Technology Ladkrabang

Ladkrabang, Bangkok 10520, Thailand

[1]Nunchanok.promsaro@wdc.com, [2]kvkasin@gmail.com, [3]pwanchai@engr.tu.ac.th

Keywords: Blocking temperature; Stripe Height; Read track width.

Abstract.

The magnetic read head technology is continuously designed to become smaller in order to get the highest areal density. Due to small volume the thermal stability is investigated for this study. The objective of this research is to study the relationship between the dimension of read head sensor and its blocking temperature. Stripe height and read track width were considered for this study. The result is blocking temperature decreasing with short stripe height. Advantage of this study is the reliability issue especially blocking temperature was captured by using resistance.

Introduction

The Hard disk drive technology is required high areal density to support the market and more demand in the long run. Consequently, the magnetic recording head has been designed to be smaller to extend the disk capacity. The technology of magnetic recording continues to progress toward higher areal density. In high areal density sensors, precision control of the track width and stripe height is required.

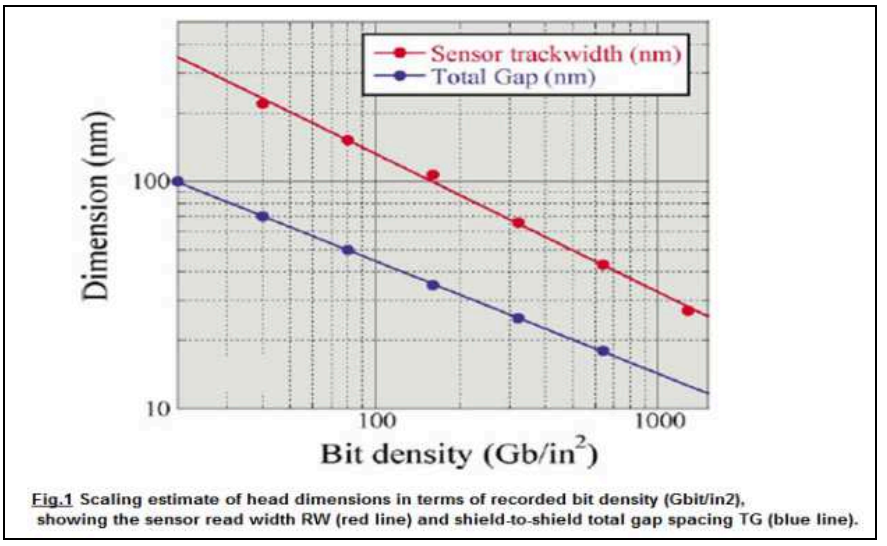

Fig.1 Scaling estimate of head dimensions in terms of recorded bit density (Gbit/in2), showing the sensor read width RW (red line) and shield-to-shield total gap spacing TG (blue line).

Figure1. *The relation between magnetic read head dimension and bit densities.[1]*

As the areal density of magnetic recording increases while the critical dimensions of recording heads have decreased. The blocking temperature (T_b) is a key parameter which depends on volume of magnetic recording read head. T_b is the temperature which the exchange bias property between an antiferromagnetic (AFM) and a ferromagnetic (FM) disappears. It correlates to the time to failure [2]. As a result, the blocking temperature is considered to be very important for reliability in magnetic recording head of hard disk drive.

Theory and Methodology

Blocking temperature

T_b testing is proposed to determine and characterize thermal noise stability which is related to reliability in read sensor head. Thermal stability in hard disk drive is extremely important, which can lead to magnetic structural degradation due to diffusion or disorder of magnetic domain in sensor heads. Figure2 shows that the magnetic domain direction in original state can be reoriented to opposite direction when temperature rises by external field stress.

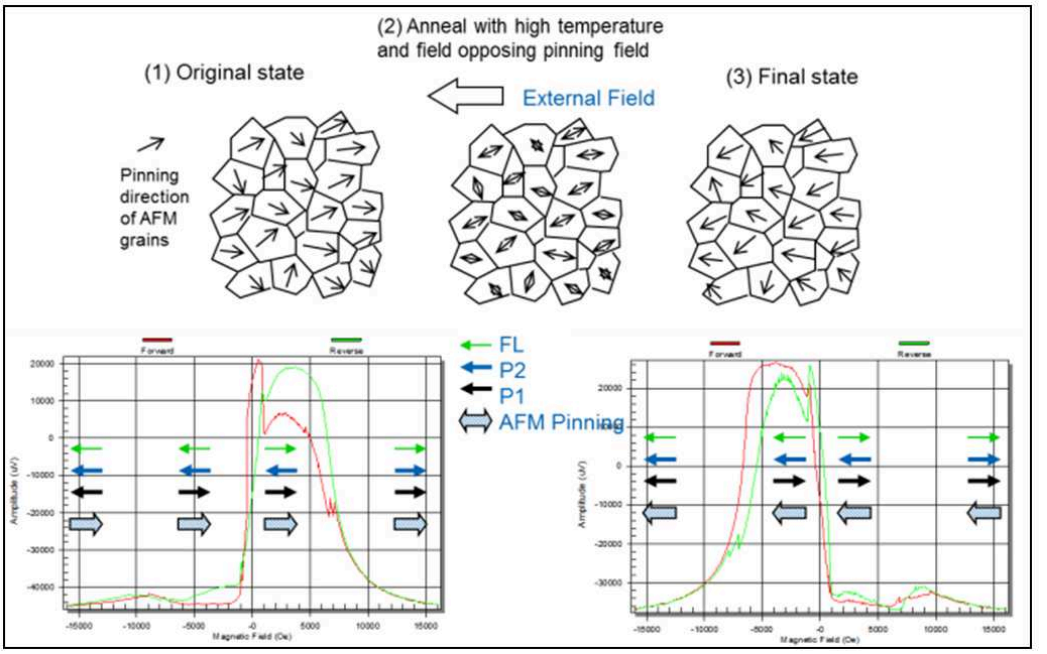

Figture2. *Temperature rises to magnetic domain direction [3]*

Many previous studies found that there are many factors impact to blocking temperature, for instant magnetic material [4], thickness of AFM layer [5], [7], ferromagnetic layer [6] and deposition condition of AFM layer [7]. The results show blocking temperature performance depends on thickness of AFM and FM layer when AFM thickness increases with decreasing thickness of FM the blocking temperature archives high performance. Another factor deposition condition, with high negative substrate biases and low pressures it yields the largest blocking temperature. Almost of those studies are in different areas from what we did in this study. Other factors especially magnetic read physical dimension such as Stripe height (SH) and Reader track width (RTW) were studied in this time.

Experiment method

The objective of this experiment is to study blocking temperature on TMR read head technology when varying SH and RTW by using Quasi Static Test machine (QST).

Blocking temperature measurement procedure

According to the pinning direction of AFM layer can be re-oriented by annealing an FM/AFM system at a temperature is greater than the blocking temperature of the AFM layer. T_b measurement procedure is as follow, apply a high magnetic field to heat up the reader, at the same time apply high field against original AFM pinning direction. Measure high frequency transfer curve (HFTC) after stress heating to see if pinning direct switched, if not increase stress voltage until AFM pinning

direction switches at stress voltage. Find the stress power at witch 50% of the pinning switched (zero net pinning) and calculate reader temperature at this stress power.

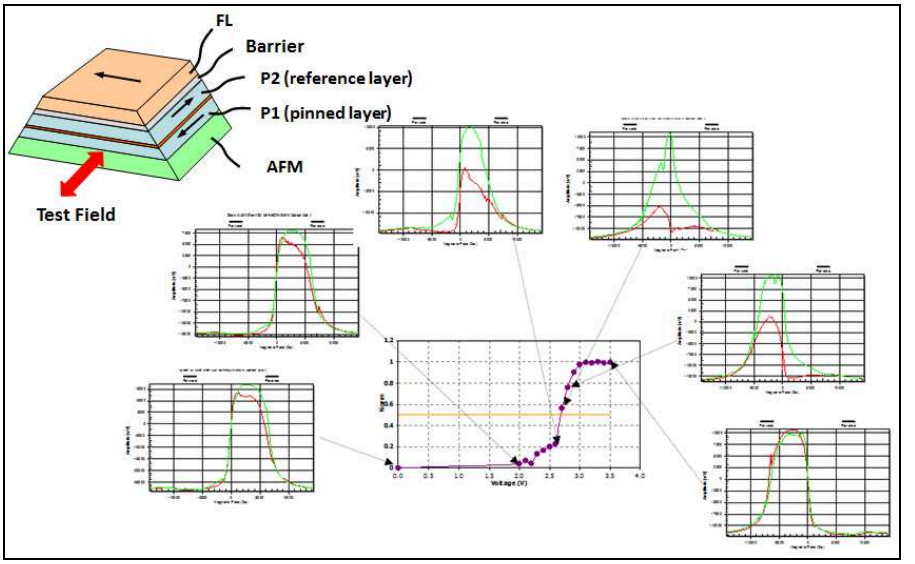

Figture3. *Diagram of blocking temperature testing [3]*

Experiment result

SH and RTW varying samples were measured blocking temperature using QST. There are 2 RTWs 24nm and 27nm. Each RTW is composed of 5 SH targets. They are a nominal SH and other 4 targets with plus and minus 10, 15 respectively.

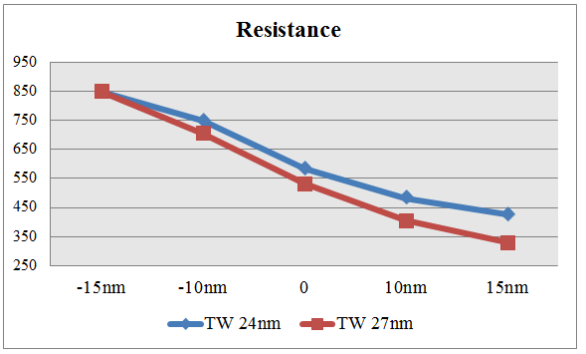

Figure4. *Resistance of each SH targets.*

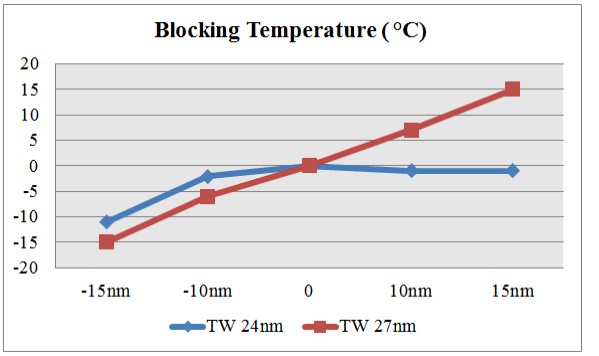

Figure5. *T_b results of each SH targets.*

Figure4 shows increasing resistances with decreasing SH for both RTWs. As expected, small magnetic read area will get high resistance. Therefor SH variation in actual manufacturing can be monitored by using resistance measurement.

Figure5 shows blocking temperature of RTW. For the 27nm, it increases with SH. The blocking temperature of the shortest SH and the longest SH is significantly lower and higher than that of the nominal SH. For narrow 24nm RTW, only the blocking temperature at the shortest SH is significant lower than that at the nominal SH. It is comparable for the longer ones.

When SH is shorter than nominal SH only 10nm (approximately about 200Ohms resistance), blocking temperature decrease by 6 °C. Therefor it can be used to detect reliability issue especially blocking temperature problem by defining the suitable resistance screening specification.

Conclusion and suggestion

The purpose of this study is to explore the magnetic read sensor performance using blocking temperature. Blocking temperature depends on reader volume, which also depends on the different in SH and RTW. In our experiment, there are 2 RTWs i.e. 24nm and 27nm. The short SHs achieve high resistance with lower blocking temperature for both RTWs. For long SHs, it shows different way. It gives low resistance with high blocking temperature only for the 27nm RTW. It is expected that the magnetic read performance is improved with higher blocking temperature. So from this study, it indicates that long SH is preferable. However areal density road map grows up with every dimensions shrink down. In facts, the need of magnetic read sensor to be small introduces some risks especially, lowering blocking temperature which will impact the reliability. To improve the magnetic read sensor performance in manufacturing, slightly long SH were considered. But this may not true for all cases, due to another RTW, the narrow 24nm, shows low blocking temperature on short SH but it does not increase even longer SH. This means that the blocking temperature cannot improve with the limitation of RTW. If RTW is too small, increasing SH will not increase the blocking temperature.

Stripe height and read track width are not only key factors for blocking temperature improvement, other factors such as pinned layer, AFM thickness and composition are also important. Further study need to be carried out to gain more understanding and improvement in read performance.

References

[1] Jeffrey R. Childress, Robert E. Fontana Jr, Magnetic recording read head sensor technology, C. R. Physique 6 (2005) 997–1012.

[2] J. P.Nozie`res,[a)] S. Jaren, Y. B. Zhang, K. Pentek, A. Zeltser,[b)] P. Wills, and V. S. Speriosu, Correlation between lifetime and blocking temperature distribution in spin-valve structures (2000).

[3] Device physic, TuMR Reader Reliability, Western Digital Corporation, Fremont CA, (2013).

[4] L. Lombard,[1,2,a] E. Gapihan,[1,2] R. C. Sousa,[1] Y. Dahmane,[1] Y. Conraux,[2] C. Portemont,[2] C. Ducruet,[2 C]. Papusoi,[1] I. L. Prejbeanu,[2] J. P. Nozières,[2] B. Dieny,[1] and A. Schuhl[1,a], IrMn and FeMn blocking temperature dependence on heating pulse width (2010)

[5] Haiwen Xia and Robert M. White and Zheng Gao and Sining Mao, Antiferromagnetic thickness dependence of blocking temperature in exchange coupled polycrystalline Ferromagnet/ Antiferromagnet bilayers. (2002)

[6] G. Vallejo-Fernandez, B. Kaeswurm, L. E. Fernandez-Outon, and K. O'Grady, Effect of the Ferromagnetic Layer Thickness on the Blocking Temperature in IrMn/CoFe Exchange Couples (2008)

[7] A. J. Devasahayama) and M. H. Kryder, The dependence of the antiferromagnet/ferromagnet blocking temperature on antiferromagnet thickness and deposition conditions.[1999]